



1 **The influence of land use and land cover change on landslide**  
2 **susceptibility: A case study in Zhushan Town, Xuanen County (Hubei,**  
3 **China)**

4 Lixia Chen<sup>1\*</sup>, Zizheng Guo<sup>2</sup>, Kunlong Yin<sup>2</sup>, Dhruba Pikha Shrestha<sup>3</sup>, Shikuan Jin<sup>4</sup>

5 <sup>1</sup>Institute of Geophysics and Geomatics, China University of Geosciences, Wuhan, 430074, China

6 <sup>2</sup>Engineering Faculty, China University of Geosciences, Wuhan, 430074, China

7 <sup>3</sup>Department of Earth Systems Analysis, Faculty of Geo-Information Science and Earth Observation (ITC), University of  
8 Twente, Enschede, 7500 AE, The Netherlands

9 <sup>4</sup>State Key Laboratory of Information Engineering in Surveying, Mapping and Remote Sensing, Wuhan University, Wuhan,  
10 430079, China

11 \*Correspondence to: Lixia Chen ([lixiachen@cug.edu.cn](mailto:lixiachen@cug.edu.cn)) Co-first author: Zizheng Guo ([cuggzz@cug.edu.cn](mailto:cuggzz@cug.edu.cn))

12 **Abstract:** Land use and land cover change can have effect on the land by increasing/decreasing landslide susceptibility  
13 (LS) in the mountainous areas. In the southwestern hilly and mountainous part of China, land use and land cover change  
14 (LUCC) has been taking place in the recent past due to infrastructure development and increase in economic activities.  
15 These development activities can also bring negative effects: the sloping area may become susceptible to landsliding due  
16 to undercutting of slopes. The study aims at evaluating the influence of land use and land cover change on landslide  
17 susceptibility at regional scale, based on the application of Geographic Information System (GIS) and Remote Sensing (RS)  
18 technologies. Specific objective is to answer the question: which land cover/land use change poses the highest risk so that  
19 mitigation measures can be implemented in time? The Zhushan Town, Xuanen County in the southwest of China was taken  
20 as the study area and the spatial distribution of landslides was determined from visual interpretation of aerial photographs  
21 and remote sensing images, as well as field survey. Two types of land use/land cover (LUC) maps, with a time interval  
22 covering 21 years (1992-2013), were prepared: the first was obtained through the neural net classification of images  
23 acquired in 1992, the second through the object-oriented classification of images in 2002 and 2013. Landslide susceptible  
24 areas were analyzed using logistic regression models. In this process, six landslide influencing factors were chosen as the  
25 landslide susceptibility indices. Moreover, we applied a hydrologic analysis method achieving slope unit (SU) delineation  
26 to optimize the partitioning of the terrain. The results indicate that the LUCC in the region was mainly the transformation  
27 from the grassland and arable land to the forest land and the human engineering activities land (HEAL). The areas of these  
28 two kind of LUC increased by 34.3% and 1.9%, respectively. The comparison of landslide susceptibility maps in various  
29 periods revealed that human engineering activities was the most important factor to increase LS in this region. Such results  
30 underline that a more reasonable land use planning in the urbanization process is necessary.



31 **Keywords:** land use and land cover change; landslide susceptibility; Geographic Information System; neural network  
32 classification; object-oriented image analysis; slope unit; logistic regression model

### 33 **1 Introduction**

34 Landslide constitutes one of the most hazardous geomorphic processes in mountain areas (Karsli et al., 2009), which can  
35 result in serious injuries, human casualties and cause physical, environmental and economic damages on a yearly basis  
36 (Fell et al., 2008; García-Ruiz et al., 2010). It is therefore necessary to take landslide hazard into account for public safety  
37 and realization of safe engineering projects (Fell et al., 2008; Gioia et al., 2015). As landslide is the results of the complex  
38 spatial-temporal interaction of many factors (Pisano et al., 2017), numerous environmental factors (e.g., slope angle, slope  
39 morphology, topography, lithology and hydrology) have been defined as the main criteria in the literature (Guzzetti et al.,  
40 2006a; Nandi and Shakoor, 2009; Pourghasemi and Rossi, 2017). Moreover, some studies have indicated that the human-  
41 induced land use and land cover change (LUCC) contributes significantly to the initiation and reactivation of landslides  
42 (Guillard and Zêzere, 2012; Galve et al., 2015; Meneses, et al., 2019), especially in populated regions, where landslides  
43 represent a major risk to human settlements, infrastructure and population (Pinyol et al., 2012; Abancó and Hürlimann,  
44 2014). So this factor should not be ignored in the process of landslide risk reduction, particularly against the background  
45 of adaptation to sustainable natural hazard risk management (Promper et al., 2015; Wang et al., 2018).

46 LUCC often imply both modifications in the natural and social systems (Promper et al., 2015; Lopez-Saez et al., 2016),  
47 in particular to changes in vegetation cover (Tasser et al., 2003; Schmaltz et al., 2017), under cutting of slopes (Scalenghe  
48 and Marsan, 2009), surface sealing or changes of drainage system (Ghestem et al., 2011, 2014), all of which potentially  
49 influence landslide hazard processes. For example, the phenomenon that mountainous areas with forest cover typically  
50 appear to be less susceptible to shallow landslides than unforested mountain slopes as described in many studies such as  
51 Curden and Miller (2001), Beguería (2006) and Galve et al. (2015). Similarly, deforestation followed by engineering  
52 activities e.g. road and/or railway construction, under cutting of slopes, development of settlement areas, buildings, etc. in  
53 steep mountainous areas increases the vulnerability to landslide hazard (Glade, 2003; Bruschi et al., 2013). All these  
54 modifications generally lead to an increase in the rate of landslide occurrences, which are strongly conditioned by land use  
55 and land cover (LUC) and hillslope morphology (Cervi et al., 2010; Piacentini et al., 2012; Reichenbach et al., 2014). These  
56 are the reasons why land use planning should be closely linked with landslide risk assessment (Glade, 2003; van Westen et  
57 al., 2006; Fell et al., 2008). For single slopes and small-scale areas, the impact of the plant root system or the spatial



58 distribution of LUC on landslides have been evaluated by various methods, including digital photogrammetric techniques  
59 (Karsli et al., 2009), microstructure analysis (Ghestem et al., 2011), laboratory shear tests (Ghestem et al., 2011), numerical  
60 modelling approaches (Mao et al., 2014) and so on. From the perspective of the regional scale, within an effective hazard  
61 mitigation planning, the landslide susceptibility (LS) is usually considered as the initial work (Chen et al., 2016; Zhou et  
62 al., 2018) which can be used to reflect the degree to which a terrain unit can be affected by future slope movements (van  
63 Westen et al., 2008; Lombardo and Mai, 2018). The importance of the influence of LUCC in landslide susceptibility  
64 analysis in regional scale, has been noted by several authors (Reichenbach et al., 2014; Pisano et al., 2017; Meneses et al.,  
65 2019).

66 During the past decades, various techniques incorporating geographical information system (GIS) along with remote  
67 sensing (RS) technologies have been widely used by researchers to map slope stability e.g. quantifying landslide hazards  
68 in relation to LUCC (Meneses et al., 2019), use of spatial statistical analysis (Kayastha, 2015), aerial photogrammetry  
69 (Karsli et al., 2009; Bruschi et al., 2013), using spaceborne optical sensors data (Taubenböck et al., 2011; Alexakis et al.,  
70 2014) and time-lapse photography for soil aggregate stability (Ymeti et al., 2017). For such studies, in general, the selection  
71 of meaningful mapping units is a basis step because it is of great importance for susceptibility zonation . A mapping unit  
72 refers to a portion of land surface with analogous geologic and/or geomorphic properties (Guzzetti et al., 2006b), which  
73 can broadly be summarized into four categories: grid cells, slope units (SU), terrain units (TU) and unique condition units,  
74 of which grid cells and SU are the most widely used (Van Den Eeckhaut et al., 2009; Rotigliano et al., 2012; Chen et al.,  
75 2016). Each category of mapping units presents advantages and disadvantages. Despite the long-term efforts by researchers,  
76 the adoption of the best mapping unit still remains a conceptual problem and an operational challenge (Guzzetti et al., 2000;  
77 Alvioli et al., 2016). In addition to the extensive discussions about this subject (Guzzetti et al., 1999; Aleotti and Chowdhury,  
78 1999; Brenning, 2005), several authors have provided examples where different mapping units were tested for the same  
79 area (Van Den Eeckhaut et al., 2009; Rotigliano et al., 2012). We can see that mostly the current trend of using grid cells is  
80 unjustified (Schlögel et al., 2018), especially considering single cell values are less representative for phenomena involving  
81 portion or whole slopes (Camilo et al., 2017); rather, a SU considers the totality of the slopes where the landslides occurred  
82 and can forecast the spatial locations of future independent landslides. As a consequence, the SU can be the correct spatial  
83 domain to operate upon.

84 In Zhushan County, land use and land cover change has been taking place in the recent past due to infrastructure  
85 development and increase in economic activities. These processes have also caused damage to the geological environment,



86 mainly in three aspects: (i) Constructions of infrastructures and residential buildings built on hillslopes, including many  
87 highways built after 2000, which resulted in the formation of steep slopes by under cutting and backfilling; (ii) Construction  
88 of mines, which led to the destruction of cultivated and forest lands. Further, due to weak awareness of environmental  
89 protection, the land restoration and treatment effects in this process are not satisfactory; (iii) As the most important water  
90 conservancy and hydropower engineering facility in the county, the Shuanglonghu Reservoir (SLHR) was built in 1992,  
91 which is located near the urban area. The change of seepage conditions caused by the dynamic change of the reservoir  
92 water level has a great impact on the stability of the slopes on both sides. The aim of our work is thus to explore the  
93 relationship between land use and land cover change and the regional landslide susceptibility. It is of utmost important to  
94 know the main land cover land use processes, which is responsible for landslide susceptibility so that preventive measures  
95 can be implement from the beginning. The study was carried out in Xuanen County, which is located in Hubei Province,  
96 China. Landslide inventory was carried out and causal factors were determined. Different LUC maps for three periods with  
97 a time interval covering 21 years (1992-2013) were prepared using remote sensing techniques. Finally, landslide  
98 susceptibility assessment was carried out in GIS environment and subsequently compared to evaluate the impact of the  
99 LUCC during this period.

## 100 **2 Methodology**

### 101 **2.1 Study area**

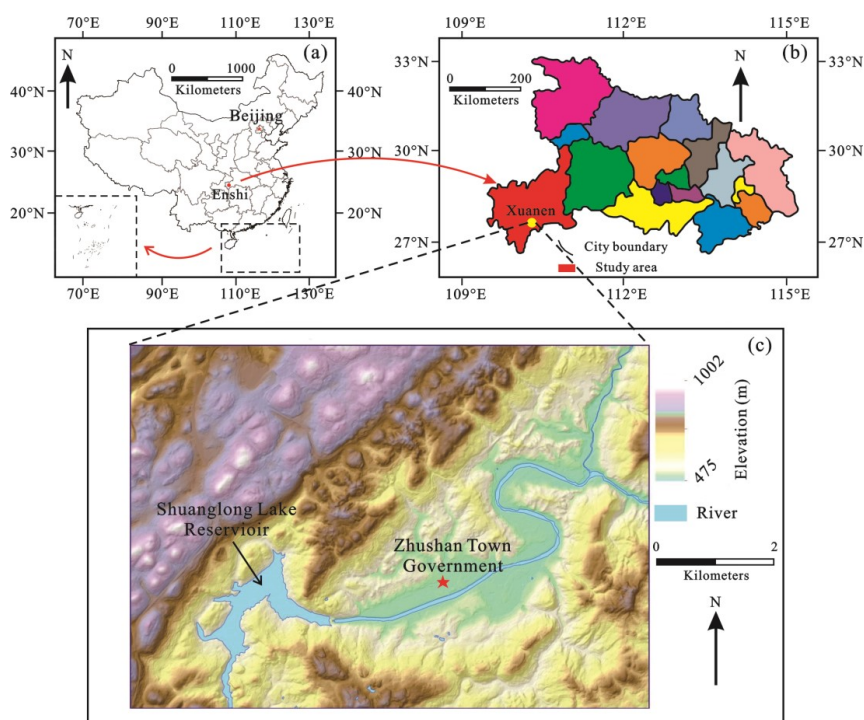
#### 102 **2.1.1 General description**

103 Xuanen County in southwest of Hubei Province (China) was selected as the study area, which is about 45 km away from  
104 the Enshi city center (Fig. 1). The study area lies within longitude 109°11'-109°55' east and latitude 29°33'-30°12' north,  
105 with surface area covering 2740 km<sup>2</sup>, among which, Zhushan Town is located in the northwestern Xuanen County with a  
106 surface area covering approximately 49 km<sup>2</sup>. The region belongs to the extension of Wuling and Qiyue Mountains and  
107 surrounded by middle and low mountains, with an elevation ranging from 350 m to 2015 m above sea level (ASL). The  
108 elevation range in most areas is 350 m - 2015 m ASL, characterized by high northwest and low southeast in the terrain.  
109 The region is located at the end of the syncline core, which spreads along the NE-SW direction. Influenced by this, the  
110 joints of NE and NW direction in the region are developed, destroying the integrity of the rock mass to some extent.

111 The climate of the study area is subtropical monsoon. Since the area is mountainous, climate can vary locally due to  
112 elevation differences. In the area with the elevation below 800 m ASL, the average annual rainfall is about 1500 mm, which



113 gradually increases with increase in elevation. When the elevation is above 1200 m ASL, the average annual rainfall  
114 exceeds 1800 mm. From the perspective of the strata, the sedimentary rocks from the Cambrian to the Cretaceous and the  
115 loose Quaternary deposits compose the strata in Xuanen County, of which the main outcropping strata consist of the Badong  
116 Formation of middle Triassic (T<sub>2</sub>b) and the Quaternary deposits. The Gongshui River is the main stream in the area, with  
117 the Shuanglong Lake Reservoir built at the upriver. Under the normal working conditions, the water level is about 490 m  
118 ASL. In the case of heavy rain or reservoir flood releasing, the water level usually increases by 1~2 m.



119  
120 **Fig. 1** The location of the study area: (a) The location of Hubei Province in China. (b) The location of Xuanen County in Hubei  
121 Province. (c) The digital elevation model (DEM) showing the basic terrain conditions

### 122 2.1.2 Urbanization and human engineering activities

123 Before the 1980s, the settlements in Xuanen County were small, with poor infrastructures and limited functions. With the  
124 rapid development of the economy in the recent past, expansion of settlement areas took place on a yearly basis, reflected  
125 by the construction of highways, in addition to the nearly doubled number of industrial and civil buildings. By early 1990s,  
126 surface area of Zhushan Town had increased significantly, of which the urban area mainly concentrated in the north side of  
127 the Gongshui River valley plain. Meanwhile, most areas surrounding the urban area were bare land or cultivated land or



128 deforested. With the constructions of infrastructures, especially along the 209 national road, the traffic condition has been  
 129 further improved and the tertiary industry (construction industry, tourism, etc.) has gradually become the pillar industry of  
 130 the area. At present, Zhushan Town has become the political and economic center of the entire county, and the urban area  
 131 has expanded on the both sides of the entire river valley plain, as well as the steep mountain areas outside the valley. The  
 132 urban area has grown from the initial 0.5 km<sup>2</sup> to nearly 7 km<sup>2</sup> (an increase of 14 times) with current population of 75000  
 133 residents, making it as one of the most densely populated towns in the county.

134 Since the main terrain condition in the study area is hilly and mountainous, the available land resources become limited.  
 135 In the process of urbanization in recent decades, many engineering activities carried out in the area have transformed the  
 136 original topography of the area by creating various levels. Although the urbanization process has improved the economic  
 137 level of the study area, the LUCC caused by construction activities has also become one of the main factors influencing  
 138 slope deformation and failure.

## 139 2.2 Data sources

140 The data used in the study mainly includes: (i) the topographic map, and (ii) the geological map for various influencing  
 141 factor maps; (iii) detailed landslide reports, (iv) aerial photographs and (v) RS images for landslide inventory map and  
 142 LUC map. Details on the data as well as details on spatial resolution and acquisition dates of satellite data are shown in  
 143 Table 1.

144 **Table 1 The sources and characteristics of the data used in the paper**

No.	Data	Scale	Resolution	Source	Purpose
1	Topographic map	1:50000	10 m	China Geological Survey (Wuhan Center)	Landslide influencing
2	Geological map	1:100000	20 m		factor maps
3	Landslide reports	/	/	China Geological Survey (Wuhan Center)	Landslide inventory
4	Aerial photographs	/	2048*1536 dpi	DJI drone	
5	Google Earth images	/	30 m	Google	map
6	RS images	/	30 m	Landsat4-5TM (28 August 1992)	LUC maps
7	RS images	/	2 m	Superview-1 (25 September 2002 And 20 September 2013)	



145 **2.3 Land use and land cover mapping**

146 Satellite remote sensing plays an important role in the earth observation (Alexakis et al., 2014) and sufficient data can be  
147 obtained for extracting land use and land cover information. The key step in this process is the RS images classification  
148 (Shrestha et al., 2019). For cases of different years, it seems to be more reasonable to use the same analysis method,  
149 especially considering the end result, which is LUC maps. Moreover, in order to make the results more accurate, the RS  
150 data quality should also be taken into account, which is mainly associated with the resolution of satellite images. In the  
151 1990s highest resolution of multispectral images was 30 m (Landsat TM), which allows optimal pixel based classification.  
152 With the development of high-resolution RS images, object-oriented techniques, using polygon entity as the basic unit,  
153 provide a widely-used method for information processing (Blaschke, 2010; Bayramov et al., 2016; Ymeti et al., 2017).  
154 Hence, for the present study both pixel-based as well as the object-oriented methods were chosen for the classifications of  
155 images in 1992, 2002 and 2013.

156 Three sets of RS images were prepared to obtain the LUC maps of different years: Landsat4-5TM images from 1992,  
157 superview-1 images from 2002 and superview-1 images from 2013. For the Landsat4-5TM images, normalized difference  
158 vegetation index (NDVI) and normalized difference water index (NDWI) were obtained using ENVI software. Then the  
159 first five bands (wavelength ranges of 0.45~0.52 $\mu\text{m}$ , 0.52~0.60 $\mu\text{m}$ , 0.63~0.69 $\mu\text{m}$ , 0.76~0.90 $\mu\text{m}$  and 1.55~1.75 $\mu\text{m}$ ,  
160 respectively) of images as well as the NDVI and NDWI were selected together for neural net classification, of which the  
161 training samples were the regions of interest determined by visual interpretation. Logistic function was determined as the  
162 activation. The number of hidden layers was set to 1 and the training rate was set to 0.5. The termination condition was set  
163 to  $10^{-4}$  and the number of training iterations was set to 500. For the superview-1 images, the multiscale segmentation was  
164 performed based on eCognition software. The parameters were set as: (i) scale parameter: 200, (ii) band weight: blue 1,  
165 Green 1 and red 1, (iii) shape: 0.6, and (iv) compactness: 0.4. Then, considering the average brightness, length-width-height  
166 ratio and shape index of the object as the features, nearest neighbor classification was carried out, where the way to obtain  
167 the ROI was similar with that in the ENVI.

168 **2.3.1 Pixel-based analysis: neural network (NN) classification**

169 NN classification aims at comparing pixels to one another and to those of known identity by using neural network algorithm,  
170 and then assigning groups of identical pixels found in remotely sensed data into classes that match the informational  
171 categories of user interest (Abdul-Qadir, 2014), so NN belongs to a supervised image classification. Numerous NN models  
172 have been developed for pattern recognition, such as (i) Hopfield networks; (ii) Hamming networks; (iii) single-layer



173 perceptron and (iv) multi-layer perceptron (MLP) (Berberoglu et al., 2000), among which BP neural network (BPNN) is  
174 the most commonly used (Aitkenhead et al., 2008). The basic element of a BPNN is the processing node and the  
175 interconnections between each node have an associated weight (Lee et al., 2004). These nodes are organized into layers,  
176 and each layer is fully interconnected to the following layer in general. Each BPNN consists of three or more interconnected  
177 layers: input layer (i.e., the first layer), output layer (i.e., the final processing layer) and hidden layer (between input layer  
178 and output layer). The number of hidden layers and nodes within each layer can be defined by the user.

179 Accurate selection of the training set is important for supervised classification. In RS images, each pixel in the image  
180 has own specific LUC information. Although mostly it is impossible to state the clear LUC characteristics of all pixels as  
181 they vary greatly, we can still determine the LUC properties of part of the pixels by statistics files, field work or known  
182 live photos. Then these pixels are considered as region of interest (ROI) and their LUC information are extracted directly  
183 from the image as the training dataset of the BPNN. This dataset is input into the nodes of the first layer and each processing  
184 node sums the values of its weighted inputs. The summed input signals are then transformed and passed to the nodes in the  
185 next layer in a feed-forward manner. After each training, the output results are compared with the actual LUC values, and  
186 the errors will be returned to the input layer for correction. Therefore, with the constant iteration of the training times, the  
187 final classification accuracy is gradually improved.

### 188 **2.3.2 Object-oriented analysis: multiscale segmentation and nearest neighbor classification**

189 The high resolution satellite imagery (HRSI) have higher spatial resolution and less spectrum number, so there are some  
190 “object with different spectra, different objects with same spectrum” phenomena (Zhang and Tang, 2019). In such images,  
191 pixels are smaller than the object so grouping of pixels is possible in order to obtain real-world homogeneous features  
192 (Blaschke, 2010; Ymeti et al., 2017). After the grouping, the smallest unit of the image in the classification process is not  
193 a pixel but the image object. It should be noted that spectral information, as well as the geometric and structural information  
194 should be all considered for subsequent analysis and processing.

195 Multiscale segmentation is a bottom-up image segmentation method based on two-two region merging techniques. It  
196 can perform multiple and continuous merging of pixels and ensure good homogeneity of all pixels in the same object of  
197 the image. There are three important parameters influencing the segmentation results: scale parameter, band weight and  
198 shape factor. The scale factor can determine the size of the object after the segmentation, as well as the final accuracy of  
199 the extracted information. The band weight can determine whether a specific band in the image is considered in the  
200 segmentation and the degree of the influence of this band. The shape factor can ensure the shape integrity of the object.





201 As a well-known commercial software to perform object-oriented analysis, eCognition (<http://www.ecognition.com/>)  
202 was selected as the tool for multiscale segmentation in this study. The supervised classification using the nearest neighbor  
203 (NN) method is used. Similar with pixel-based analysis, this method allows to select region of interest (ROI) for taking  
204 training samples. In addition, it allows the description of samples in terms of shape and texture of the objects in the feature  
205 space. The classification of the test object is determined by the nearest neighbor. The distance between the test and sample  
206 objects can be calculated as follows:

$$207 \quad l = \sqrt{\sum_f \left( \frac{v_f^{(t)} - v_f^{(s)}}{\sigma_f} \right)^2} \quad (1)$$

208 where  $f$  is the order of the feature,  $v_f^{(t)}$  is the feature values of the test object,  $v_f^{(s)}$  is the feature values of the sample  
209 object, and  $\sigma_f$  is the standard deviation of the feature.

#### 210 **2.4 Logistic regression model**

211 Numerous models have been developed to perform landslide susceptibility assessment, which could be divided into four  
212 categories: heuristic, deterministic, statistical and machine learning models (Huang et al., 2017). Considering that the  
213 objective of our study is to observe the impact of LUCC in terms of their propensity to landslide initiation, a single mul-  
214 tivariate statistical classification model is suitable. For this purpose, we prepared the logistic regression model (LRM) to  
215 link the dependent variable expressing landslide probability with the independent variables (landslide influencing factors).

216 For landslide susceptibility assessment, logistic regression is a commonly used statistical technique that involves one  
217 or more independent explanatory variables to extract the empirical relationships from observations (Zhou et al., 2018). It  
218 helps the researchers to model the presence or absence probability of a certain event according to the values of the predictor  
219 variables that they observed (Ozdemir et al., 2013). In particular, through the addition of a suitable link function to the  
220 usual linear regression model, variables in the model may be either continuous or discrete, or any combination of both  
221 types and that they do not necessarily have normal distributions (Lee, 2005), which gives it an advantage over linear and  
222 log-linear regressions. Ozdemir et al (2013) and Lee (2005) have explained the detailed formula in the case of landslide  
223 susceptibility studies, which is denoted as follows:

$$224 \quad Y = a + b_1 X_1 + b_2 X_2 + b_3 X_3 + \dots + b_m X_m \quad (2)$$

$$225 \quad Y = \log \text{it} (P) = \ln \left( \frac{P}{1-P} \right) \quad (3)$$



226 
$$p = \frac{e^y}{1 + e^y} \quad (4)$$

227 where  $X_1, X_2, \dots, X_m$  are predictor variables and  $Y$  is a linear combination function of these variables that represent a linear  
228 relationship. If  $Y$  is used as a binary variable (0 or 1), then the value 0 or 1 represent the absence or presence of a landslide,  
229 respectively; The parameters  $a, b_1, b_2, \dots, b_m$  are the regression coefficients that must be estimated, among which is the  
230 intercept, and  $b_1, b_2, \dots, b_m$  are the coefficients that measure the contribution of the independent variables ( $X_1, X_2, \dots, X_m$ ) to  
231 the variations in  $Y$ ;  $P$  is the probability that the target variable ( $Y$ ) is 1;  $P/(1-P)$  is the so-called odd or frequency ratio.  
232 Through this process, the model can establish a function relationship between binary coded landslide events and the  
233 different factors used for landslide susceptibility assessment (Yalcin et al., 2011).

234 After the analysis of the relationship between the landslide and the predictor variables, the value of  $P$  can be considered  
235 as the landslide susceptibility index ( $LSI$ ). There are many methods for  $LSI$  classification, such as natural breaks, equal  
236 intervals and standard deviations (Huang et al., 2017). In this study, the  $LSIs$  were divided into four classes e.g. very high,  
237 high, moderate and low, according to the reasonable thresholds of  $LSI$  determined by natural breaks method.

### 238 2.5 Receiver operating characteristic (ROC) curve

239 Although the statistical methods can evaluate the model performance effectively such as the frequency ratio ( $FR$ ) index,  
240 they require reclassification of landslide susceptibility index ( $LSI$ ) values, and the change of the different breakpoint values  
241 can result in various evaluation results. Hence, this kind of methods are also called cutoff-dependent approaches (Zhou et  
242 al., 2018). To remedy this, ROC curve is more commonly used to evaluate landslide susceptibility results due to the cutoff-  
243 independence of it.

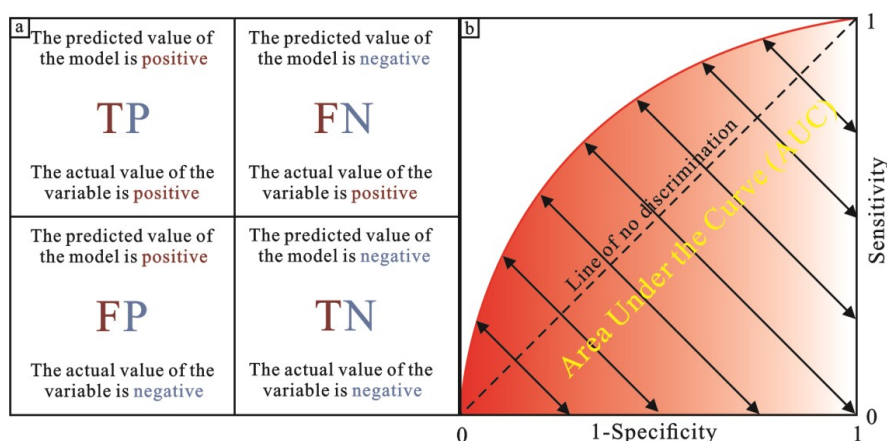
244 Several indices (Fig. 2 (a)) are proposed to evaluate landslide-prone area classification in ROC method, including true  
245 positive (TP) rate, true negative (TN) rate, false positive (FP) rate, false negative (FN) rate, sensitivity and specificity. In  
246 simple terms, if a model predicts a positive value of a given variable (event forecast) and the value of the variable is actually  
247 positive (event), a TP prediction is obtained. On the opposite, if the value of the variable is actually negative (no event), a  
248 FP prediction is obtained (Corsini and Mulas, 2017). TN and FN predictions are classified following similar logical  
249 combinations. Based on this, the sensitivity (Sen), i.e., the percentage of correctly classified landslide cases, and the  
250 specificity (Spe) can be determined as follows:

251 
$$Sen = \frac{\text{"Number of TP"}}{\text{"Number of TP"} + \text{"Number of FN"}} \quad (5)$$

252 
$$Spe = \frac{\text{"Number of TN"}}{\text{"Number of FP"} + \text{"Number of TN"}} \quad (6)$$



253 The Sen is also considered as the true positive rate and the value  $(1 - \text{Spe})$  is the rate of false positives (Melchiorre et  
 254 al., 2008). Generally, High sensitivity indicates a high number of correct predictions whereas high specificity (low 1-Spe  
 255 difference) indicates a low number of false positives (Mohammady et al., 2012). Hence, the Sen of the model is plotted  
 256 against 1-Spe to obtain the ROC curve, and in most cases, the area under the curve (AUC) is utilized to evaluate the  
 257 prediction ability of models, and the model is considered better if the value of AUC is larger (Fig. 2 (b)).



258  
 259 **Fig. 2 (a) Some indices used to evaluate the landslide susceptible area classification in ROC method; (b) The example of ROC**  
 260 **and AUC (source: Corsini and Mulas, 2017).**

## 261 2.6 Slope unit

262 Slope unit (SU) was applied as the basic spatial domain as it considers the totality of the slopes where the landslides  
 263 occurred. A SU is defined as one slope part, or the left/right part of a watershed, representing the region of space delimited  
 264 between ridges and valleys under the constraint of homogeneous slope aspect and steepness distributions. It can avoid the  
 265 shortcomings of low geomorphological representativeness of grid-based susceptibility mapping (Camilo et al., 2017).  
 266 Hence, we adopted the SU as the mean to research landslide susceptibility in this study.

267 The SU can be drawn manually from topographic maps of adequate scale and quality or it can be delineated  
 268 automatically using specialized software (Alvioli et al., 2016). According to the prevalent methods provided by the  
 269 literature (Xie et al., 2004; Reichenbach et al., 2014; Schlögel et al., 2018), the SUs of the study area were partitioned using  
 270 ArcGIS-based hydrologic analysis method where SUs were the hydrological terrain subdivision bounded by drainage and  
 271 divide lines. Slope units were generated as follows: (i) preparing the reverse DEM by subtracting the original DEM from  
 272 the highest elevation of the study area; (ii) filling the original and the reverse DEM, respectively; (iii) extracting the surface  
 273 water flow direction to distinguish areas with extremely rapid changes in surface morphology; (iv) establishing the stream



274 link for obtaining the valley lines and ridge lines; (v) delineating the SUs based on the valley and ridge lines. One of the  
275 advantages of adopting slope units is that the computational burden is reduced due to lower number of units compared with  
276 the grid-based method (Camilo et al., 2017). Moreover, the SUs makes it possible to maximize the internal homogeneity  
277 and the external heterogeneity of the slope aspect (Mashimbye et al., 2014; Schlögel et al., 2018).

## 278 **2.7 Landslide mapping and analysis**

### 279 **2.7.1 Landslide mapping**

280 As the simplest form of landslide mapping, landslide inventory plays a very essential role in landslide susceptibility  
281 (Kayastha, 2015), especially in the initial phase of LS assessment because it provides the spatial distribution of locations  
282 of existing landslides (Tian et al., 2019). It can be done in a region using different techniques such as field survey, satellite  
283 image/air photo interpretation, and literature search for historical landslide records (Yalcin et al., 2011). The inventory was  
284 carried out from a combination of: (i) detailed reports from management institutes, (ii) visual interpretation of aerial  
285 photographs and remote sensing images, and (iii) field surveys carried out in the period from April to May 2013. To clarify  
286 the detailed landslide information, the landslide property database was also linked to the map, which includes the  
287 descriptions of some data that cannot be digitized, such as the amount, area and occurrence time of landslides and so on.

### 288 **2.7.2 Factors influencing landslides**

289 The spatial distribution of landslide hazards is the combined consequence of different factors, including not only internal  
290 geological backgrounds but also the external environmental settings. In this work, six influencing factors were determined  
291 first for LS analysis, i.e., slope, aspect, slope shape, lithology, distance to reservoir and LUC. Therefore, different thematic  
292 data on these factors are needed to prepare a LS map (Kayastha, 2015). These data are collected from different sources.  
293 For example, elevation contour lines (1:50000 scale) and the geological map (1:100000 scale) were obtained from China  
294 Geological Survey, which were used for the extraction of topographic factors (i.e., slope, aspect and slope shape) and  
295 geological factors (i.e., lithology). The urban planning map, recording the detailed location of Shuanglonghu Reservoir,  
296 was collected from the government of Zhushan Town. The LUC maps were obtained from RS images.

297 The analysis for the relationship between landslide events and their triggering factors is a key step in landslide  
298 susceptibility assessment. In this study, this relationship was determined by the calculation of the ratio of the amount of  
299 units with landslide occurrence to the total amount of units in each class, namely the distribution curve of ratio. It should  
300 be noted that the original continuous variables (e.g., slope, aspect, etc.) cannot be input directly into the used model. in



301 order to obtain a general knowledge about the effects of the variable on landslide occurrence, it is necessary to discretize  
302 these variables into subclasses according to the distribution curve of the frequency ratios (Huang et al., 2017). Moreover,  
303 after the selection and preliminary analysis of these factors, the conditional independence among them was tested. The  
304 results showed that all the variables were irrelevant due to the correlation coefficient of less than 0.2, so it is appropriate to  
305 take these factors into account for landslide susceptibility.

### 306 *Topographic factors*

307 From the elevation contour lines with intervals of 10 m, a digital elevation model (DEM) of the study area was prepared.  
308 Based on this DEM, topographic factors including slope, aspect and slope shape were obtained.

309 Slope angle (Fig. 3 (a)), defined as the steepness of a surface, is the major parameter of slope stability analysis which  
310 can help us understand the characteristics of a basin for runoff and erosion processes (Vasu and Lee, 2016). The slope  
311 angle of the study area varies greatly, with a range of  $0^{\circ}$ ~ $73.6^{\circ}$  and an average value of  $21.3^{\circ}$ . The continuous slope angles  
312 were divided into four categories: (i) flat to gentle slope ( $<15^{\circ}$ ); (ii) moderate slope ( $15$ - $25^{\circ}$ ); (iii) steep slope ( $25$ - $40^{\circ}$ ); (iv)  
313 very steep slope ( $>40^{\circ}$ ). From the perspective of spatial distribution, the flat to gentle slope angle mainly appears along the  
314 banks of the Gongshui River, while the surrounding mountains are steeper with the slope angle mainly varying from  $20^{\circ}$   
315 to  $45^{\circ}$ . Based on the statistical results of LRM, the landslides mainly occurred in the moderate slope because its regression  
316 coefficient values was the largest among all the categories.

317 Aspect (Fig. 3 (b)) is also considered an important factor in landslide susceptibility assessment because many  
318 parameters in relation to aspect may affect the occurrence of landslides, such as exposure to sunlight, winds, rainfall (degree  
319 of saturation), and discontinuities (Yalcin et al., 2011). The aspect of this study was divided into seven categories. The  
320 statistical results revealed that the landslide is the easiest to occur on the aspect of  $40$ - $100^{\circ}$  in all three years. Moreover,  
321 the categories of aspect, which have a positive effect in the occurrence of landslides are in the range of  $100$ - $120^{\circ}$  and  $260$ -  
322  $300^{\circ}$ , respectively.

323 Defined along the line of maximum slope, profile curvature (Fig. 3 (c)) affects the acceleration and deceleration of  
324 flow and, therefore, influences subsequent erosion and deposition (Regmi et al., 2010). However, the geological meaning  
325 of the profile curvature is not obvious. To remedy this, we classified the profile curvature map into three categories  
326 according to the values of the slope profile curvature: (i) convex; (ii) concave; (iii) straight (planar). These categories  
327 represent different slope shapes. In general, concave slopes are considered as potentially landslide-prone areas as they  
328 concentrate water at the lowest point, that can contribute to develop adverse hydrostatic pressure whereas convex slopes



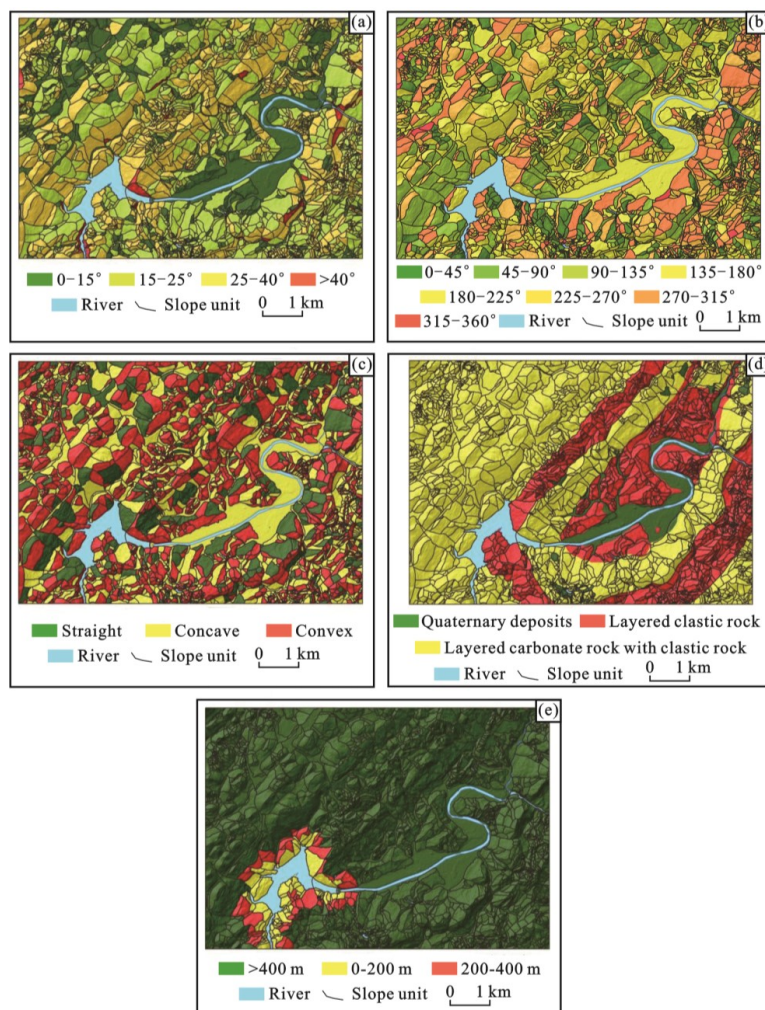
329 are more stable because they disperse the runoff more equally down the slope (Kayastha, 2015). This point can be confirmed  
330 by the model used in this study.

### 331 ***Lithology***

332 As a component of the geomorphological research, the landslide event has a close relationship with the lithological  
333 characteristics of the land, because different rocks have different mechanical and hydrological properties (Van Westen et  
334 al., 2008). The lithology map (Fig. 3 (d)) of the study area was extracted from the geological map (1:100000 scale), which  
335 indicated that the main strata of Zhushan Town consist of Jianglingjiang Formation (T<sub>1j</sub>) of lower Triassic (northwest of  
336 the urban area), Badong Formation (T<sub>2b</sub>) of middle Triassic (most areas of the region) and the Quaternary deposits (banks  
337 of the Gongshui River). From the perspective of the material types, the T<sub>2b</sub> is a kind of clastic rock composed of marine-  
338 terrigenous interdepositional mudstone, siltstone and marl (Deng et al., 2017), and the T<sub>1j</sub> is a kind of carbonate rock  
339 composed of marine depositional dolomite, dolomitic limestones and microcrystalline limestone. Similarly, the Quaternary  
340 deposits also have several components, such as alluvium, proluvium and so on. Hence, according to the characteristics of  
341 engineering geology, these strata was differentiated into three lithological units: (i) the Quaternary deposits; (ii) layered  
342 clastic rock; (iii) layered carbonate rock with clastic rock. With the largest regression coefficient, the category of (ii) shows  
343 the strongest positive impact on the occurrence of landslides. More than 80% landslides developed in the stratum of layered  
344 clastic rock, although the amount of units of this category only accounts for 38.3% of the total units, which indicates that  
345 Badong Formation is a landslide-prone stratum.

### 346 ***Distance to reservoir***

347 The large-scale engineering infrastructures can damage the initial geological conditions so that the slope stability is also  
348 influenced. In areas with abundant runoff, reservoir construction is the most common infrastructure development to make  
349 full use of water resources, but it also has been classified a significant factor inducing landslides (Iqbal et al., 2018), such  
350 as the Three Gorges Reservoir in China (Huang et al., 2017; Wang et al., 2018; Zhou et al., 2018). In order to see the effect  
351 of the Shuanglonghu Reservoir on landsliding, the distance to reservoir map (Fig. 3 (e)) was prepared, with a buffer distance  
352 of 200 m. Then, the study area was divided into three categories: (i) < 200 m; (ii) 200-400 m; (iii) > 400 m. We can see that  
353 although the area of the category of (i) and (ii) only accounts for about 5% of the whole region, the ratio of the units with  
354 the occurrences of landslide is larger than the category of (iii).



355  
356 **Fig. 3 Influencing factors used in the landslide susceptibility modelling: (a) slope angle; (b) aspect; (c) profile curvature; (d)**  
357 **lithology; (e) distance to reservoir.**

358 ***Land use and land cover***

359 It is well known that different LUC types may control the stability of slopes, of which the mechanism can be clarified by  
360 an amount of hydrological and mechanical effects, including changing hydrological functioning of hillslopes, affecting  
361 rainfall partitioning, infiltration characteristics, and runoff production, and even the shear strength of the soil (García-Ruiz  
362 et al., 2010). At the same time, different from several environmental factors such as geological structure and lithology,  
363 which are considered constant over a long period, the LUC can be affected by major modifications seasonally or over a  
364 period of decades because it can be natural or induced and controlled by human actions (Reichenbach et al., 2014). Hence,



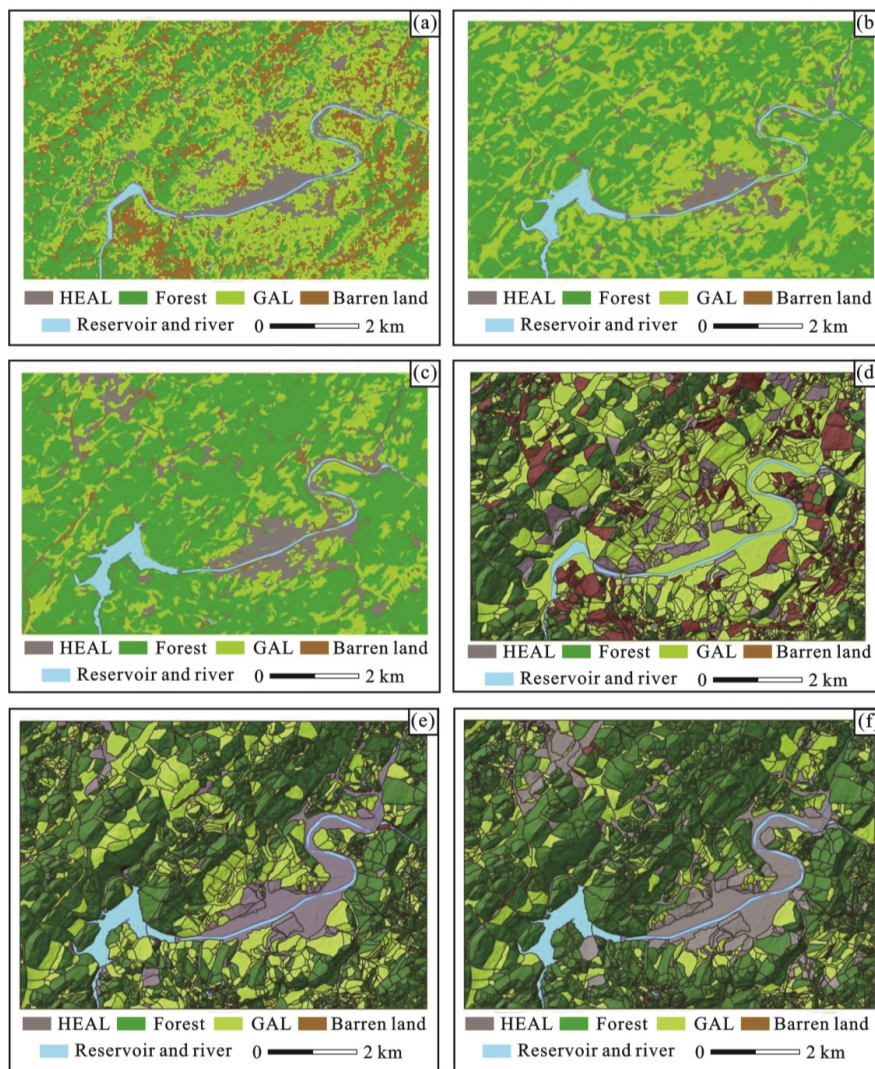
365 for a region where the LUC types can change obviously over a relatively short period, the correlation between LUC type  
366 and landslides should be defined to assess the effect of LUC on the occurrence of landslides. For the LUC maps the  
367 evolution over time must be extracted through the comparison from at least two different time periods (Pisano et al., 2017).  
368 In this study, a time interval covering 21 years (1992-2013) was considered, which were divided into two ranges: 1992-  
369 2002 and 2002-2013. It should be noted that the maps before 1992 was not provided because of the availability of the RS  
370 images needed for the mapping procedure and the undeveloped urbanization at that time.

### 371 **3. Results**

#### 372 **3.1 Land use and land cover maps**

373 In the process of classification, although various LUC types were identified from the RS images, some of the types were  
374 later combined for statistical analysis. For example, the lands for urban buildings, roads and mines were all combined and  
375 defined as the human engineering activities land (HEAL). Both of the grassland and arable land (GAL) are the shallow  
376 surface of the ground covered by certain vegetation, so they were considered as the same LUC type. Finally, the LUC map  
377 (Fig. 4 (a), (b) and (c)) of the study area was classified into four classes: (i) human engineering activities land; (ii) forest;  
378 (iii) grassland and arable land; (iv) barren land. The data were then integrated in an ArcGIS environment where 2870 slope  
379 units have been delineated according to the method in 3.4 section. Finally, the characteristics of spatial distribution of  
380 different LUC types were indicated based on slope units (Fig. 4 (d), (e) and (f)). The classification accuracies of different  
381 years were evaluated by confusion matrix showed in the Table 2 and some evaluation indices were used such as producer's  
382 accuracy (PA) and user's accuracy (UA). Overall, all of the classification results are good with the overall accuracies (OA)  
383 approximately 90% or more than 90%. In addition, for a single LUC type, most of the PAs and UAs are larger than 80%,  
384 indicating the type was identified successfully, especially the results of 1992, which has the accuracies of larger than 90%  
385 for nearly all of the evaluation indices. Such results can provide a solid base for landslide susceptibility assessment.  
386





387

388

389

Fig. 4 (a) The LUC map of 1992; (b) The LUC map of 2002; (c) The LUC map of 2013; (d) The LUC map of 1992 based on SU; (e) The LUC map of 2002 based on SU; (f) The LUC map of 2013 based on SU.

390

391

392

393

394

395

396

397

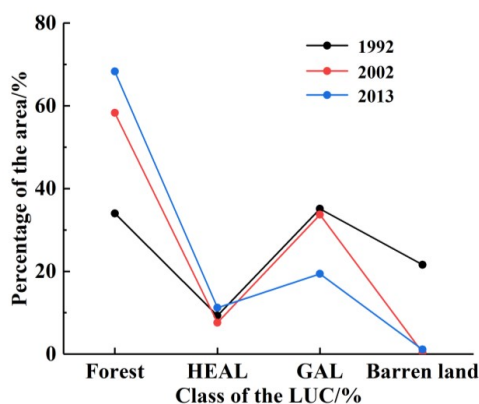


398

**Table 2 The classification accuracies of LUC maps for different years**

Year	LUC	PA/%	UA/%	OA/%	Kappa/%
1992	HEAL	98.4	99.5		
	Forest	95.8	97.2		
	GAL	91.5	85.2	95.6	93.9
	Barren land	94.5	97.5		
2002	HEAL	87.8	90		
	Forest	88.1	94.9		
	GAL	100	96.4	92.3	88.8
	Barren land	83.3	62.5		
2013	HEAL	87.5	87.5		
	Forest	100	100		
	GAL	89.2	97.1	89.3	83.4
	Barren land	91.7	73.3		

399 As seen in Fig. 5, from 1992 to 2013, the area of barren land has decreased obviously, mainly because the urbanization  
 400 process has been continuing, leading to most of barren land was used for other purposes, such as human buildings, roads  
 401 and so on. Similarly, the change of the grassland and arable land also shows the characteristic of rapid reduction. Contrary  
 402 to this, the areas of the category of (i) and (ii) increased in this period, especially the forest land, with the percentage among  
 403 the total area increasing from 34% in 1992 to 68.3% in 2013. Even though most studies have revealed that regional forest  
 404 degradation was more likely to occur in the past decades (Karsli et al., 2009; García-Ruiz et al., 2010; Galve et al., 2015),  
 405 obviously, it was not the case in our paper. In fact, some studies still support such results like ours, despite their driving  
 406 forces to cause the increase of forest are different, such as depopulation and land abandonment (Beguería, 2006), conscious  
 407 landscape management (Pisano et al., 2017) and so on. In this work, the increase of forest is mainly beneficial from two  
 408 points: (i) the phenomenon of deforestation before 1992 was serious, causing a large number of natural forests disappeared.  
 409 With the enhancement of awareness of environmental protection in the area, especially after the year of 2000, the  
 410 environment problems have gradual been the focused issue by the decision-makers of China. National policy of "returning  
 411 farmland to forest" performed since 1999 has produced a very positive results. (ii) The development of tourism industry,  
 412 which calls for a better ecological environment.



413

414 **Fig. 5** The change of area of different land use and land cover types.

### 415 **3.2 Landslide inventory**

416 The inventory (Fig. 6) revealed 53 landslides in the area, of which 1 occurred in the period 1992-2002, and 10 occurred  
417 during 2002 to 2013. The total area of these landslides is  $201.6 \times 10^4 \text{ m}^2$ , with a volume of approximately  $1000 \times 10^4 \text{ m}^3$ .

418 According to the type of movement, material (Cruden and Varnes 1996) and estimated depth, most of the them are shallow  
419 earth slides, and composite soil slide–debris flows. The deformation of many landslides are characterized by cracks (Fig.

420 7), including tension and bulging cracks on the ground, and deformation cracks on the buildings. For some landslides in

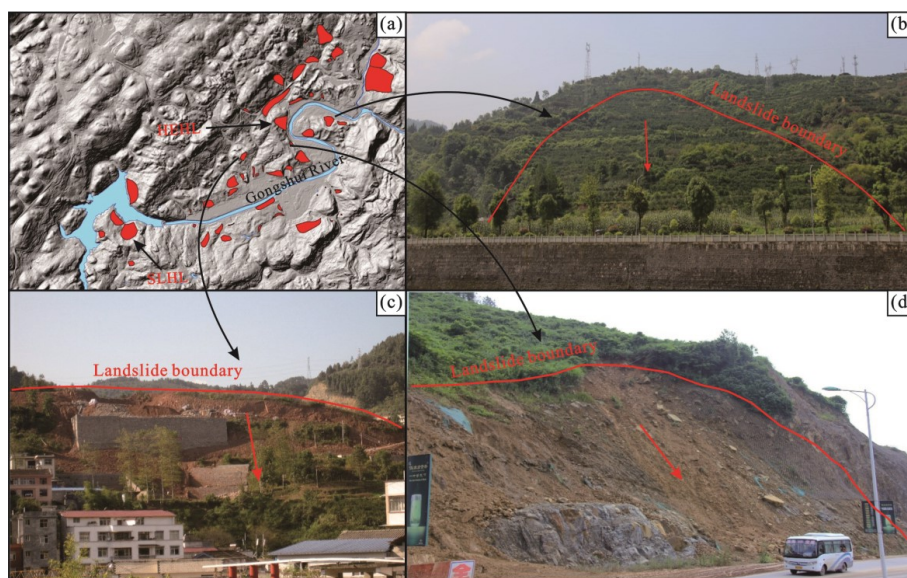
421 the urban area, strong slope cutting cause the small-scale sliding on the toe of them. For example, the Huanghexiang

422 landslide (HHXL), located 500 m on the northwest side of the Qingshui River, is a shallow earth slide, which develops on

423 the slide-prone strata of the Badong Formation (Deng et al., 2017). Under the combined effects of strata and slope cutting,

424 HHXL was induced with many cracks observed, causing serious threat to residents.

425



426

427 **Fig. 6** The spatial locations of the landslides and the photos of different types of landslides in the study area: (a)The spatial  
 428 locations of the landslides. (b)The photo of the rock slide. (c) The photo of the composite soil slide–debris flows. (d) The photo of  
 429 the shallow earth slide.



430

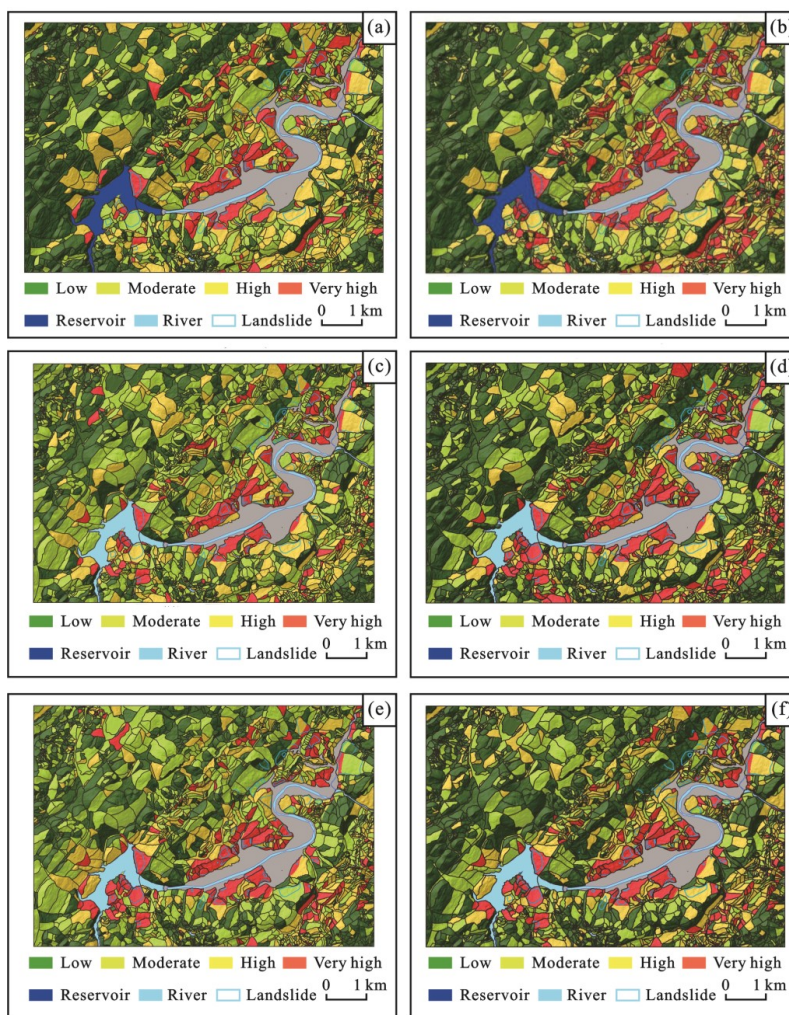
431 **Fig. 7** The deformation of the landslides in the study area: (a) The topography of SLHL (see Fig. 6 (a) for location). (b)The cracks  
 432 on the road of SLHL. (c) The uplift of the ground of SLHL. (d) The topography of HEHL (see Fig. 6 (a) for location). (e) The  
 433 tension cranks of the ground on HEHL. (f) The cracks of the building of HEHL.

### 434 3.3 Landslide susceptibility zonation

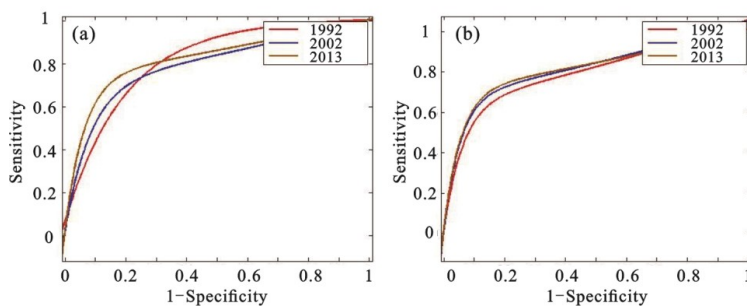
435 Landslide susceptibility maps obtained by logistic regression model are showed in Fig. 8 (a), (c) and (e). Meanwhile, the  
 436 weight of evidence model (Regmi et al., 2014; Razavizadeh et al., 2017) was utilized as the comparison model (Fig. 8 (b),



437 (d) and (f)). The ROC curves were applied to show the success accuracies of different models qualitatively, by plotting the  
438 cumulative percentage of observed landslide occurrence against the cumulative percentage from very high to low  
439 susceptibility with decreasing *LSI* values. As shown in the Fig. 9 and Table 3, in all six cases, all of the AUC values are  
440 larger than 80% (except the result of 2002 by weight of evidence model), showing good accuracies of the landslide  
441 susceptibility assessment. Through comparing the results of different models in the same year, we can see that the logistic  
442 regression model is better than weight of evidence model in this work. Especially, the change of ROC curves, sensitivity  
443 and specificity values of weight of evidence model in different periods are more obvious. For instance, the sensitivity  
444 values are 83.0%, 70.8% and 79.9%, respectively, while that of logistic regression model are 74.6%, 75.0% and 78.4%,  
445 respectively, indicating that the performance of logistic regression model is more stable than that of weight of evidence  
446 model.



447  
 448 **Fig. 8** The results of landslide susceptibility zonation: (a) LRM for 1992; (b) WEM for 1992; (c) LRM for 2002; (d) WEM for  
 449 2002; (e) LRM for 2013; (f) WEM for 2013.



450  
 451 **Fig. 9** The ROC curves of (a) WEM, and (b) LRM



452

453

**Table 3 The accuracies of different models**

Model	Year	True positive	True negative	False positive	False negative	Sensitivity	Specificity	AUC
		rate/%	rate/%	rate/%	rate/%	%	%	%
Weight of evidence model	1992	1.4	66.2	32.1	0.3	83.0	67.3	81.3
	2002	1.2	76.7	21.6	0.5	70.8	78.0	78.8
	2013	1.7	73.9	24.0	0.4	79.9	75.5	82.0
Logistic regression model	1992	1.2	74.1	24.3	0.4	74.6	75.3	81.8
	2002	1.3	75.9	22.4	0.4	75.0	77.2	84.0
	2013	1.6	72.8	25.1	0.5	78.5	74.7	81.8

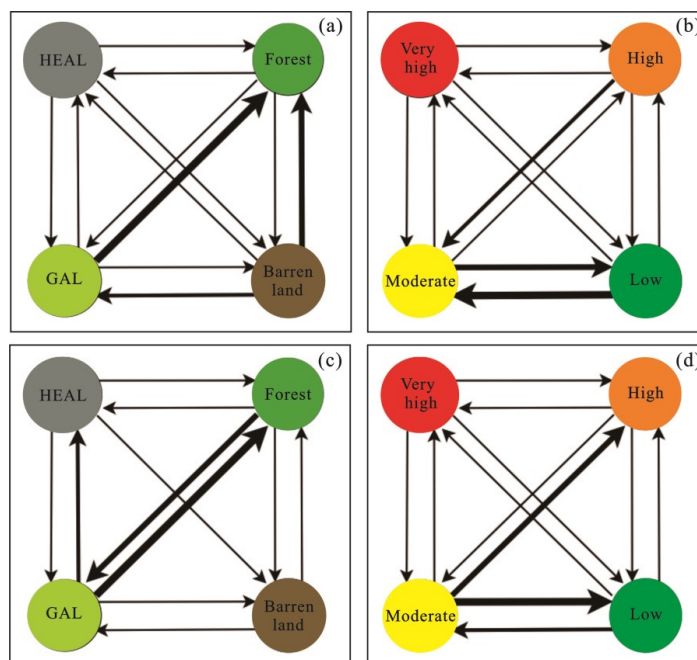
454 **3.4 Evolutions of LUC and landslide susceptibility**

455 After the preparation of mappings, the LUC and landslide susceptibility of the same locations in different periods were  
 456 placed together to compare so that it is possible to clarify the evolutions of LUC and LS with a time interval covering 21  
 457 years. It should be noted that logistic regression model had been clarified to have a better performance for landslide  
 458 susceptibility in this study, so the subsequent analysis was carried out in the framework of this model.

459 As seen in Fig. 10, in the period of 1992 – 2002, the main trend of LUCC is that the arable land transfer into forest  
 460 and the barren land transfer into arable land and forest, especially the area of barren land decreased, from the percentage  
 461 of 19.8% in 1992 to 0.2% in 2002. In contrast, the forest increased by the percentage of 33.6%. Except the reasons stated  
 462 in the 5.1 section, the data quality should also be considered: the low-resolution images of Landsat4-5TM lead to bad  
 463 classification between barren land and grassland covered by sparse vegetation. Contrary to these two types of LUC, the  
 464 human engineering activities land did not change obviously in the area and amount of units. This is mainly because the  
 465 urbanization process during this period concentrated on the plain areas on the banks of the valley, which always belonged  
 466 to one slope unit with large area due to the flat terrain. In the environmental conditions mentioned above, compared with  
 467 1992, the landslide susceptibility of 1227 units in the study area has changed in 2002 (Fig. 11), among which the landslide  
 468 susceptibility of 632 units increased and that of 595 units decreased, accounting for 22.0% and 20.7%, respectively, of the  
 469 amount of total slope units. Further, If the magnitude of the landslide susceptibility changes are subdivided into five classes:  
 470 obvious increase (LS has increased by at least two levels, e.g., from low to high), increase, constant, decrease and obvious

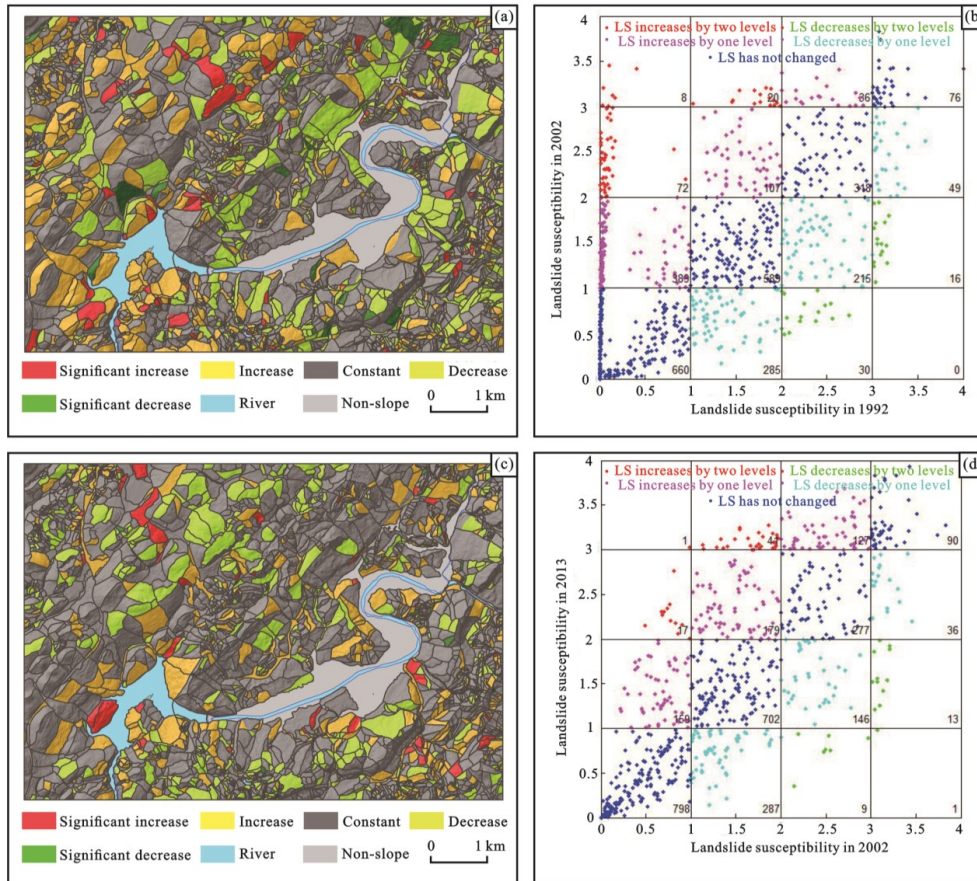


471 decrease (LS has decreased by at least two levels), it can be seen that similar with the overall change of landslide  
472 susceptibility, the amount of the units of obvious increase is also larger than that of obvious decrease. Such characteristics  
473 of LS change indicate that the LUCC from 1992-2002 made Zhushan Town a more landslide-prone area. Then, the LUCC  
474 of the units with obvious increase LS was analyzed. The LUCC under this condition can be summarized into three cases:  
475 (i) constant, (ii) human engineering activities land transferred from other types of LUC, and (iii) grassland and arable land  
476 transferred from other types of LUC. The amounts of the units of these three cases are 24, 36 and 40, respectively, which  
477 reveals that there are two important types of LUC for increasing LS in this period: increase of the human engineering  
478 activities land, and the transformation from forest to grassland and arable land. Moreover, it is worth mentioning that in  
479 these units with obvious increase LS, none unit transfers from the human engineering activities land to other types,  
480 indicating that the impact of human engineering activities on the LUC is generally decisive so that the landslide  
481 susceptibility is hardly to change due to the internal influence to the geological conditions.



482  
483 **Fig. 10 (a) The transformation of LUC from 1992 to 2002; (b)The transformation of LS from 1992 to 2002; (c)The transformation**  
484 **of LUC from 2002 to 2013; (d)The transformation of LS from 2002 to 2013.**





485  
 486 **Fig. 11 (a) The change of the landslide susceptibility of each slope unit between 1992 and 2002; (b) The scatter plot showing the**  
 487 **change of the landslide susceptibility between 1992 and 2002; (c) The change of the landslide susceptibility of each slope unit**  
 488 **between 2002 and 2013; (d) The scatter plot showing the change of the landslide susceptibility between 2002 and 2013.**

489 In the period of 2002 – 2013, the trend of LUCC mainly includes two aspects (Fig. 10): the first is the slightly  
 490 increase of the human engineering activities land, mainly from the transformation of the grassland and arable land. Different  
 491 from the previous period, the human engineering activities during this period were no longer confined to the plain areas on  
 492 the banks of the valley, but carried out on the other areas, such as the northwestern part of the county. Similar situation also  
 493 happened in the southeast of the county. Both areas were mainly covered by the forest and the grassland and arable land  
 494 before. The second is the increase of the forest. Interestingly, the mutual transformation of forest and grassland and arable  
 495 land also can be seen such as the northeast of the region. This indicates that orderly and reasonable land use planning was  
 496 gradually developed in this region. In other words, the focused point by the residents is not the increase of the area of the  
 497 forest anymore, but the accurate place where the forest should be planted. This is a further manifestation of the enhancement



498 of the people's awareness of environmental protection. As a result, the land around the town in 2013 was mainly covered  
499 by forest, not by the arable land like in the 2002. Such land use planning can effectively protect the town from the harsh  
500 environment problems (e.g., sandstorm, flood). Under such conditions of LUCC, the landslide susceptibility of 947 units  
501 has changed in 2013 (Fig. 11), among which the landslide susceptibility of 441 units increased and that of 506 units  
502 decreased, accounting for 15.4% and 17.6%, respectively, of the total units. Compared with 2002, all of these numbers are  
503 smaller, indicating that the influence of the LUCC during this period was slighter than that during 1992-2002. The units of  
504 obvious increase and obvious decrease for landslide susceptibility in 2013 were 59 and 23, respectively, also smaller than  
505 that in 2002. The LSs of most units were constant during this period. This is mainly because (i) the increase of the human  
506 engineering activities land was small, and (ii) the impact of forest and grassland and arable land on the stability of the land  
507 was limited. Despite this, the change of landslide susceptibility influenced by the human engineering activities land is still  
508 obvious. During this period, a total of 195 units were transformed from other types of LUCC to the human engineering  
509 activities land, of which the landslide susceptibility of 161 units increased and none of units had a reduced LS. Among the  
510 total 59 units with obviously increased LS, the LUC of 46 units were transformed to the human engineering activities land,  
511 accounting for 78.0 % of the total units. Hence, the transformation to this type of LUCC played an important role in the  
512 increase of the landslide susceptibility in the region, mainly because the slope cutting in the engineering activities  
513 influenced internal geological conditions and necessary measures were not implemented due to the lack of professional  
514 knowledge.

### 515 **3.5 Typical landslide events influenced by LUCC**

516 In the period during 2002~2013, 9 landslide events occurred in the study area, among which 2 are located at the bank of  
517 the SLHR, mainly triggered by the reservoir water level. Hence, the remaining landslides were taken as the examples to  
518 explore the impact of the engineering activities on land. A 25m buffer of each landslide was established and then the change  
519 of the engineering activities in the buffer was counted. Except one landslide, the area of the engineering activities around  
520 all landslides have expanded since 2002. Overall, the average range of engineering activities around the landslides have  
521 increased by nearly 20%, and the change mainly focused on the toe of the landslides, indicating that the under cutting of  
522 slope is common in the region.

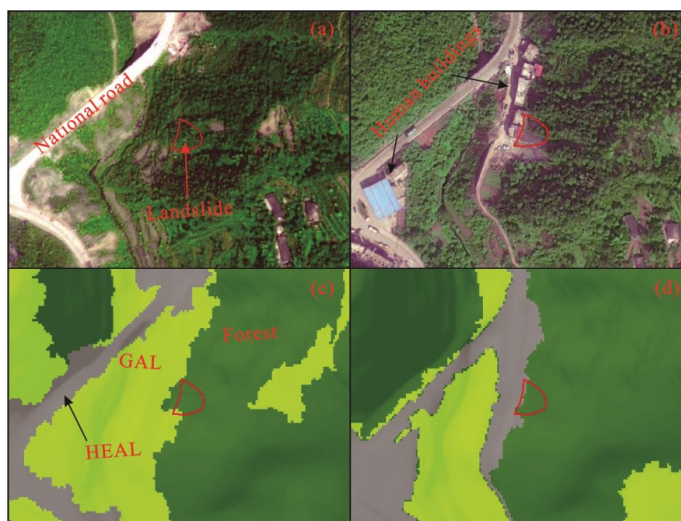
#### 523 **3.5.1 The Qili Bridge Landslide (QLQL)**

524 The QLQL (Fig. 12) located at Qili Bridge village of the Zhushan County, on the right side of the national road G209. The



525 slope where the landslide developed had an elevation ranging from 520 m to 762 m above the sea level (ASL) and a gully  
526 with a strike direction of  $340^\circ$  existed in the toe of the slope. The QLQL developed at the lower part of the slope, with an  
527 area of  $9000 \text{ m}^2$  and a volume of  $0.27 \times 10^4 \text{ m}^3$ . The landslide is a semicircular-shape in plane and a straight line in profile.  
528 The landslide materials mainly composed of cataclastic marl rock of Triassic and Quaternary deposits including silty clay  
529 and rubble soil.

530 In 2007, at the lower part of the slope, where the elevation was approximately 520 m ASL, a platform began to be  
531 constructed, and then 6 brick-and-concrete buildings with 3–4 storeys were built on the platform without any protection  
532 measures. The slope was a consequent bedding rock slope with a natural dip angle more than  $30^\circ$ . The steep free surface  
533 with a height of about 3 m was caused by the slope excavation. Combined with the rather cataclastic materials of the QLQL  
534 with many fissures, the rainfall infiltrated into the sliding body rapidly, making the strength of the materials gradually  
535 reduced. In July 2011, the continuous heavy rain induced the landslide. The back walls of the buildings were destroyed by  
536 the rock mass, causing some injuries and severe economic losses. As seen in Fig. 12, before the construction of the buildings,  
537 the natural slope was mainly covered by the forest land, grassland and arable land. However, the subsequent engineering  
538 activities disrupted the original geological conditions, causing the instability of the slope. Even nowadays, some sliding  
539 materials still remain on the slope, being a big potential danger for the residents.



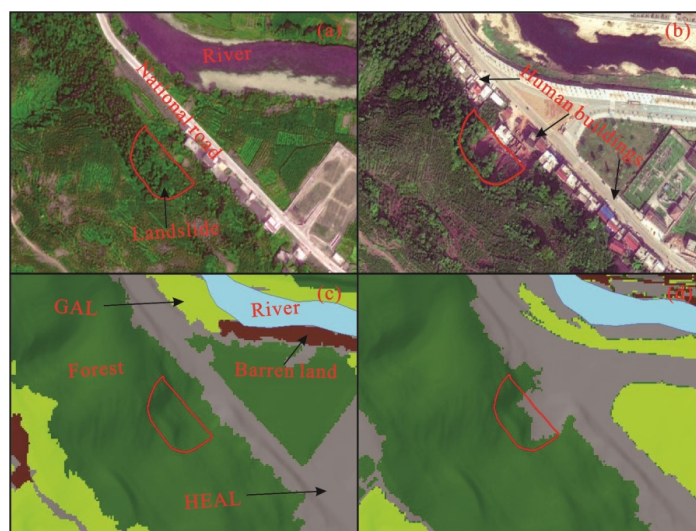
540  
541 **Fig. 12** The LUCC around the QLQL: (a) The RS image of QLQL in 2002 (obtained from Superview-1 RS data); (b) The RS  
542 image of QLQL in 2013 (obtained from DJI drone); (c) The LUC type of QLQL in 2002; (d) The LUC type of QLQL in 2013.



543 **3.5.2 The Liangshuigou Landslide (LSGL)**

544 The LSGL (Fig. 13) located at Lianhuaba village, on the left bank of the Gongshui River. The natural slope had a dip angle  
545 ranging from  $25^{\circ}$ ~ $35^{\circ}$  with a slope aspect of  $55^{\circ}$ . The LSGL developed at the lower part of the slope, with an area of 6300  
546  $m^2$  and a volume of  $0.1 \times 10^4 m^3$ . The landslide is an irregular-shape in plane and step-like in profile. The landslide materials  
547 mainly composed of the Quaternary deposits including silty clay and rubble soil. The bedrock was mainly argillaceous  
548 siltstone of Badong Formation in Triassic with developed joints and fissures, which cut the rock mass into blocks.

549 Before 2010, the slope was mainly covered by citrus trees and crops (arable land). However, with the progress of the  
550 urbanization, many human engineering activities were performed in the nearby area, including the constructions of the  
551 building and the road. The slope cutting at the toe of the slope caused a free surface with a height of about 10 m. On June  
552 2012, the landslide was triggered by the heavy rainfall event.



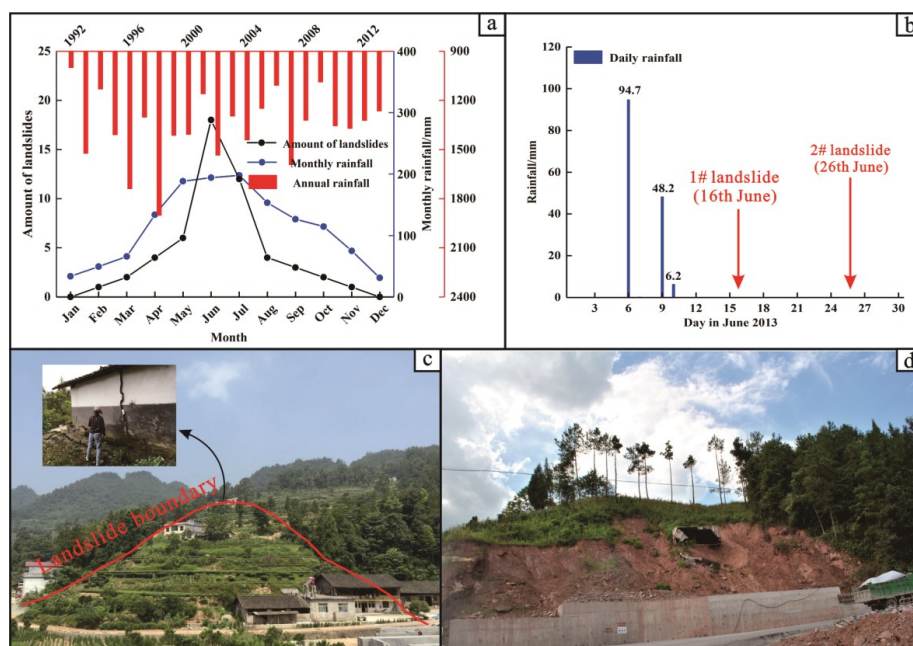
553  
554 **Fig. 13 The LUCC around the LSGL: (a) The RS image of LSGL in 2002 (obtained from Superview-1 RS data); (b) The RS**  
555 **image of LSGL in 2013 (obtained from DJI drone); (c) The LUC type of LSGL in 2002; (d) The LUC type of LSGL in 2013.**

556 **4. Discussion**

557 Although the results highlight the significance of LUCC in the susceptibility assessment of shallow landslides, it is obvious  
558 that LUCC is not the only factor that can influence the landslide occurrence in the region. In fact, in most cases, the impact  
559 of LUC on landslides is about the internal geological conditions, such as terrain features, drainage conditions, even stress  
560 field distribution. Such impacts can worsen/improve the stability of natural slopes to increase/decrease the landslide areal



561 frequency in these zones (Schmaltz et al., 2017 Galve et al., 2015). For instance, a case study in the Spanish Pyrenees by  
562 Begueria (2006) has verified that due to the water redistribution in the slopes after prolonged rainfall periods, the former  
563 arable fields on the valley slopes still facilitated landsliding, even after land abandonment and revegetation by shrubs or  
564 trees. However, it should be noted that the shallow landslides are directly triggered by the LUC, except some landslides  
565 induced by slope cutting effect. The statistical results of the temporal distribution of landslides in this study area also  
566 support this assumption: the positive correlation between the number of landslides and monthly average rainfall (statistical  
567 result of daily rainfall data between 1992~2013) is rather strong. The amount of landslides occurring in June and July are  
568 18 and 12, respectively, accounting for 56.6% of the total landslides, whereas only 10 landslides did not occur in the rainy  
569 season (May ~ September), accounting for 18.9% of the total landslides. Based on this, from the perspective of the period  
570 with a 21-year interval, the change of the landslide susceptibility at regional scale is associated with rainfall conditions. As  
571 seen in Fig. 14, the overall annual rainfall between 1992 and 2013 first increases (1992~1998) and then decreases  
572 (1999~2013), although the magnitude of the change is relatively slight. Similar patterns are also showed in the amount of  
573 heavy rainfall events of this period. It should be noted that this law is roughly the same as the change of the high  
574 susceptibility area. Thus, to be exact, it's not that the LUCC can change the susceptibility directly, but the natural slope  
575 conditions are influenced by various LUC and subsequently show different environments for the landslides development.  
576 In conclusion, most landslides in the area, especially shallow landslides, were not triggered by a single factor, but the  
577 combined results of external environmental factors. For example, two landslides (i.e., 1# and 2# landslides) occurred in the  
578 period from 16<sup>th</sup> to 26<sup>th</sup> in June 2013, triggered by a heavy rainfall event with a total rainfall of 149.1 mm from 6<sup>th</sup> to 9<sup>th</sup>.  
579 However, if a longer time scale is taken into account, the role that human engineering activities play also become very  
580 important, because many engineering activities including buildings and road constructions were performed on the locations  
581 of these two landslides a few years ago.



582

583 **Fig. 14** The relationship between rainfall and shallow landslides in the area: (a) The curve showing monthly rainfall and temporal  
584 distribution of landslides; (b) Daily rainfall in June 2013; (c) The topography of 1# landslide; (d) The topography of 2# landslide.

585 In addition, the fluctuation of the reservoir water level is also a triggering factor that cannot be ignored. The SLHL is  
586 the appropriate example. Before the construction of the reservoir (1992), the slope unit where the landslide is located has  
587 moderate susceptibility, whereas it increased to very high susceptibility level in 2002 and 2013. Although the reservoir is  
588 also a kind of human engineering activities, this landslide was mainly triggered by the reservoir impoundment. Seasonal  
589 and periodic fluctuation of the reservoir water level affects the seepage conditions of inside the landslide and soften the  
590 geotechnical properties, both of which can gradually worsen the landslide stability. The field survey has captured the  
591 appearance of a large amount of cracks on the ground of SLHL after the construction of the reservoir. A nearly decade of  
592 deformation observation also indicated the slow but continuous movement of the landslide, with a velocity of  
593 approximately 1.6m/yr. In particular, the landslide movement shows an obvious intermittent characteristic: the movement  
594 accelerates in the rainy season in which period the reservoir water level generally decreases, while the movement often  
595 stops in other periods. Obviously, the landslide is undergoing the creep deformation influenced by the reservoir water level  
596 combined with rainfall. In the final analysis, however, this kind of impact was not highlighted because the reservoir area  
597 was considered as a kind of HEAL, leading that the change of the susceptibility of this slope unit was incorporated into the  
598 results of LUCC. To remedy this, specific analysis for single landslide is necessary to completely understand the triggering



599 mechanism of the landslide, but this is not the case in our work. Hence, it can be seen that due to the limitation of the  
600 estimation model, availability of the data, and scale of the study, the impact of LUCC on landslides in this paper was  
601 partially exaggerated, especially in areas where various triggering factors (e.g., HEA, rainfall, reservoir water level, etc.)  
602 may exist at the same time.

603 In order to explore the impact of LUCC on landslide occurrence, it is believed that in this work the temporally and  
604 spatially differentiated information for both, landslide inventory and LUC maps are particularly important to be considered,  
605 while the other used influencing factors were considered as static factors. However, they have proven to be dynamic, with  
606 changes occurring even in few decades. Especially, in populated areas, the topographic factors (i.e., slope angle, aspect and  
607 profile curvature in this work) can be greatly altered by frequent earth surface movement processes (e.g., landslides, soil  
608 erosion, slope cutting, etc.) in a short time. Hence, a more accurate susceptibility result calls for good timeliness of initial  
609 DEM data and influencing factor maps, which in fact is seldom available, at least for an undeveloped area in the 1990s.  
610 Moreover, in landslide susceptibility evaluation, the LUC data integrate the controlling factor group and, generally, are  
611 directed by another factor input to the evaluation model. In some cases, LUC data are used as a landslide conditioning  
612 factor, which is usually scarce, generalized and not very detailed (Meneses et al., 2019). For instance, the CORINE land  
613 cover (CLC) data are widely used for landslide assessment in many regions of Europe because it is the only LUC data  
614 available (Feranec et al., 2007). A similar situation happens in the analysis of 1992 in this study. The RS data with low  
615 resolution caused the inherent uncertainties of the obtained LUC maps, which was subsequently taken into the landslide  
616 susceptibility model. Even though we have tried to reduce such uncertainties by decreasing the amount of LUC categories  
617 and using classification method of images with better accuracy, the final LS zonation results were still related with  
618 considerable uncertainties. Under this condition, it seems not to be important to compare different models to improve the  
619 accuracy of landslide susceptibility evaluation. For example, Schmaltz et al. (2017) have recommend to apply easily  
620 interpretable multi variable model or generalized additive models that allow to include potential confounders for similar  
621 studies, which is in accordance with the model used in our study.

## 622 **5. Conclusion**

623 Land use and land cover change can alter the geological conditions and affect the occurrence of the landslides. This study  
624 is to observe the evolution of LUC and detail the effects of LUC change on landslide susceptibility at a regional scale.  
625 Zhushan County in Hubei Province (China), a landslide-prone area, was taken as the study area. Through the analysis of



626 different LUC maps with a time interval covering 21 years obtained from remote sensing images, we documented the rapid  
627 growth of the afforestation as well as intense urbanization process in this region since 1990s: the areas of forest land and  
628 human engineering activities between 1992 and 2013 increased by 34.3% and 1.9%, respectively; whereas the areas of the  
629 grassland and arable land, and the barren land decreased by 15.7% and 20.5%, respectively. Combined with other five  
630 factors (slope angle, aspect, profile curvature, lithology and distance to reservoir), the LUC was subsequently utilized for  
631 landslide susceptibility analysis in different years based on logistic regression model and slope unit. The zonation results  
632 revealed that the urban area on both sides of the river valley plain is always the area with the largest landslide susceptibility.  
633 Along with the increase of engineering construction activities, the susceptibility of many areas increases. Even some small  
634 shallow landslides were directly triggered by the transformation of LUC type (i.e., from forest and GAL to HEAL) because  
635 original geological conditions were disrupted in this process.

636 Overall, the RS images with good resolution and the appropriate model for landslide susceptibility are the keys to  
637 evaluate the impact of land use and land cover change on landslide susceptibility. Although the resolution of RS images  
638 used in 1992 is not accurate enough, some evaluation indices still show a good classification accuracy of LUC maps. In  
639 addition, as a result of this study, it can be shown that human activities play an important role on the change of landslide  
640 susceptibility. Any engineering activities in the sloping area could pose landslide hazard if mitigation measures are not  
641 considered and implemented from the beginning. Consequently, the method used in the present work provides important  
642 benefits for landslide hazard mitigation efforts due to the combined use of both GIS and RS techniques. Such results not  
643 only call for a more reasonable land use planning in the urbanization process in the future, but also suggest a more  
644 systematic inclusion of LUC change in hazard assessment.

645 **Data availability.** The study relied on three sets of data: (i) the data collected by the field work, (ii) remote sensing data,  
646 and (iii) the detailed landslide investigation reports provided by China Geological Survey (Wuhan Center). The categories  
647 (i) and (2) are included in Table 1 in this paper. The detailed processing workflow for these data sets can be seen in the  
648 methodology section of this paper. Unfortunately, the regional-scale geological data is not available because this is not  
649 allowed by the rules of China Geological Survey (Wuhan Center).

650 **Author contribution.** Yin and Chen led the field work and data collection. Jin prepared the remote sensing data and  
651 processed the RS images. Chen and Guo discussed the research plan and prepared the paper together. Guo carried out the  
652 statistical analysis and prepared the figures of the paper. Chen supervised the project and Shrestha helped in the paper





653 development and English writing. So Chen and Guo contributed equally and they were listed as co-first authors of the paper.

654 **Competing interests.** The authors declare that they have no conflict of interest.

655 **Special issue statement.** This article is part of the special issue “Natural hazards impacts on technological systems and  
656 infrastructures”. It is not associated with a conference.

657 **Acknowledgements.** This work was financed by the project “Studies on spatial-temporal differences of large accumulation  
658 landslide deformation and its vulnerability model for buildings in the Three Gorges reservoir” (No. 41877525) funded by  
659 the National Natural Science Foundation of China.

660 **References:**

661 Abancó, C., and Hürlimann, M.: Estimate of the debris-flow entrainment using field and topographical data, Nat. Hazards,  
662 71, 363-383, <https://doi.org/10.1007/s11069-013-0930-5>, 2014.

663 Abdul-Qadir, A. M.: Supervised classification for lithologic discrimination in Shaikh Ibrahim area, NW Iraq using Landsat  
664 images, Arab. J. Sci. Eng., 39, 437-451, <https://doi.org/10.1007/s13369-013-0911-8>, 2014.

665 Aitkenhead, M. J., Flaherty, S., and Cutler, M. E. J.: Evaluating neural networks and evidence pooling for land cover  
666 mapping, Photogramm. Eng. Remote Sens., 8, 1019-1032, <https://doi.org/10.14358/PERS.74.8.1019>, 2008.

667 Aleotti, P., and Chowdhury, R. N.: Landslide hazard assessment: summary review and new perspectives, Bull. Eng. Geol.  
668 Environ., 58, 21-44, <https://doi.org/10.1007/s100640050>, 1999.

669 Alexakis, D. D., Grillakis, M. G., Koutroulis, A. G., Agapiou, A., Themistocleous, K., Tsanis, I. K., Michaelides, S.,  
670 Pashiardis, S., Demetriou, C., Aristeidou, K., Retails, A., Tymvios, F., and Hadjimisis, D. G.: GIS and remote sensing  
671 techniques for the assessment of land use change impact on flood hydrology: the case study of Yialias basin in Cyprus,  
672 Nat. Hazards Earth Syst. Sci., 14, 413-426, <https://doi.org/10.5194/nhess-14-413-2014>, 2014.

673 Alvioli, M., Marchesini, I., Reichenbach, P., Rossi, M., Ardizzone, F., Fiorucci, F., and Guzzetti, F.: Automatic delineation  
674 of geomorphological slope units with r. slope units v1.0 and their optimization for landslide susceptibility modeling,  
675 Geosci. Model Dev., 9, 3975-3991, <https://doi.org/10.5194/gmd-9-3975-2016>, 2016.

676 Bayramov, E., Buchroithner, M., and Bayramov, R.: Quantitative assessment of 2014–2015 land-cover changes in  
677 Azerbaijan using object-based classification of LANDSAT-8 timeseries. Model. Earth Syst. Environ., 2, 35-47,



- 678 <https://doi.org/10.1007/s40808-016-0088-8>, 2016.
- 679 Berberoglu, S., Lloyd, C. D., Atkinson, P. M., and Curran, P. J.: The integration of spectral and textural information using  
680 neural networks for land cover mapping in the Mediterranean, *Comput. Geosci.*, 26, 385-396,  
681 [https://doi.org/10.1016/S0098-3004\(99\)00119-3](https://doi.org/10.1016/S0098-3004(99)00119-3), 2000.
- 682 Begueria, S.: Changes in land cover and shallow landslide activity: a case study in the Spanish Pyrenees, *Geomorphology*,  
683 74, 196-206, <https://doi.org/10.1016/j.geomorph.2005.07.018>, 2006.
- 684 Blaschke, T.: Object based image analysis for remote sensing, *ISPRS. J. Photogramm. Remote Sens.*, 65, 2-16,  
685 <https://doi.org/10.1016/j.isprsjprs.2009.06.004>, 2010.
- 686 Brenning, A.: Spatial prediction models for landslide hazards: review, comparison and evaluation, *Nat. Hazards Earth Syst.*  
687 *Sci.*, 5, 853-862, <https://doi.org/10.5194/nhess-5-853-2005>, 2005.
- 688 Bruschi, V. M., Bonachea, J., Remondo, J., Gómez-Arozamena, J., Rivas, V., Barbieri, M., Capocchi, S., Soldati, M., and  
689 Cendrero, A.: Land management versus natural factors in land instability: some examples in northern Spain, *Environ.*  
690 *Manage.*, 52, 398-416, <https://doi.org/10.1007/s00267-013-0108-7>, 2013.
- 691 Camilo, D. C., Lombardo, L., Mai, P. M., Dou, J., and Huser, R.: Handling high predictor dimensionality in slope-unit-  
692 based landslide susceptibility models through LASSO-penalized Generalized Linear Model, *Environ. Model Softw.*,  
693 97, 145-156, <https://doi.org/10.1016/j.envsoft.2017.08.003>, 2017.
- 694 Cervi, F., Berti, M., Borgatti, L., Ronchetti, F., Manenti, F., and Corsini, A.: Comparing predictive capability of statistical  
695 and deterministic methods for landslide susceptibility mapping: a case study in the northern Apennines (Reggio Emilia  
696 Province, Italy), *Landslides*, 7, 433-444, <https://doi.org/10.1007/s10346-010-0207-y>, 2010.
- 697 Chen, L., van Westen, C. J., Hussin, H., Ciurean, R. L., Turkington, T., Chavarro-Rincon, D., and Shrestha, D. P.: Integrating  
698 expert opinion with modelling for quantitative multi-hazard risk assessment in the Eastern Italian Alps,  
699 *Geomorphology*, 273, 150-167, <https://doi.org/10.1016/j.geomorph.2016.07.041>, 2016.
- 700 Corsini, A., and Mulas, M.: Use of ROC curves for early warning of landslide displacement rates in response to precipitation  
701 (Piagneto landslide, Northern Apennines, Italy), *Landslides*, 14, 1241-1252, <https://doi.org/10.1007/s10346-016-0718-8>, 2017.
- 702
- 703 Cruden, D. M., and Varnes, D. J.: Landslide types and processes. In: Turner, A. K. , Schuster, R. L. (eds) *Landslides,*  
704 *investigation and mitigation. Transportation Research Board Special Report 247.* Transportation Research Board,  
705 Washington DC, pp 36-75, 1996.



- 706 Deng, Q., Fu, M., Ren, X., Liu, F., and Tang, H.: Precedent long-term gravitational deformation of large scale landslides in  
707 the Three Gorges reservoir area, China, *Eng. Geol.*, 221, 170-183, <https://doi.org/10.1016/j.enggeo.2017.02.017>, 2017.
- 708 Fell, R., Corominas, J., Bonnard, C., Cascini, L., Leroi, E., and Savage, W. Z.: Guidelines for landslide susceptibility,  
709 hazard and risk zoning for land use planning, *Eng. Geol.*, 102, 85-98, <https://doi.org/10.1016/j.enggeo.2008.03.022>,  
710 2008.
- 711 Feranec, J., Hazeu, G., Christensen, S., and Jaffrain, G.: Corine land cover change detection in Europe (case studies of the  
712 Netherlands and Slovakia), *Land use policy*, 24, 234-247, <https://doi.org/10.1016/j.landusepol.2006.02.022>, 2007.
- 713 Galve, J. P., Cevasco, A., Brandolini, P., and Soldati, M.: Assessment of shallow landslide risk mitigation measures based  
714 on land use planning through probabilistic modelling, *Landslides*, 12, 101-114, <https://doi.org/10.1007/s10346-014-0478-9>, 2015.
- 716 García-Ruiz, J. M., Beguería, S., Alatorre, L. C., and Puigdefábregas, J.: Land cover changes and shallow landsliding in  
717 the flysch sector of the Spanish Pyrenees, *Geomorphology*, 124, 250-259, <https://doi.org/10.1016/j.geomorph.2010.03.036>, 2010.
- 719 Ghestem, M., Sidle, R. C., and Stokes, A.: The influence of plant root system on subsurface flow: implications for slope  
720 stability, *Bioscience*, 61, 869-879, <https://doi.org/10.1525/bio.2011.61.11.6>, 2011.
- 721 Ghestem, M., Veylon, G., Bernard, A., Vanel, Q., and Stokes, A.: Influence of plant root system morphology and  
722 architectural traits on soil shear resistance, *Plant Soil.*, 377, 43-61, <https://doi.org/10.1007/s11104-012-1572-1>, 2014.
- 723 Glade, T.: Landslide occurrence as a response to land use change : a review of evidence from New Zealand, *Catena*, 51,  
724 297-314, [https://doi.org/10.1016/S0341-8162\(02\)00170-4](https://doi.org/10.1016/S0341-8162(02)00170-4), 2003.
- 725 Gioia, E., Carone, T., and Marincioni, F.: Rainfall and land use empirically coupled to forecast landslides in the Esino river  
726 basin, central Italy, *Nat. Hazards Earth Syst. Sci.*, 15, 1289-1295, <https://doi.org/10.5194/nhess-15-1289-2015>, 2015.
- 727 Guzzetti, F., Carrara, A., Cardinali, M., and Reichenbach, P.: Landslide hazard evaluation: a review of current techniques  
728 and their application in a multi-scale study, Central Italy, *Geomorphology*, 31, 181-216, [https://doi.org/10.1016/S0169-555X\(99\)00078-1](https://doi.org/10.1016/S0169-555X(99)00078-1), 1999.
- 730 Guzzetti, F., Cardinali, M., Reichenbach, P., and Carrara, A.: Comparing landslide maps: a case study in the upper Tiber  
731 River Basin, central Italy, *Environ. Manage.*, 25, 247-263, <https://doi.org/10.1007/s002679910020>, 2000.
- 732 Guzzetti, F., Galli, M., Reichenbach, P., Ardizzone, F., and Cardinali, M.: Landslide hazard assessment in the Collazzone  
733 area, Umbria, Central Italy, *Nat. Hazards Earth Syst. Sci.*, 6, 115-131, <https://doi.org/10.5194/nhess-6-115-2006>,



- 734 2006a.
- 735 Guzzetti, F., Reichenbach, P., Ardizzone, F., Cardinali, M., and Galli, M.: Estimating the quality of landslide susceptibility  
736 models, *Geomorphology*, 81, 166-184, <https://doi.org/10.1016/j.geomorph.2006.04.007>, 2006b.
- 737 Guillard, C., and Zêzere, J.: Landslide susceptibility assessment and validation in the framework of municipal planning in  
738 Portugal: the case of Loures Municipality, *Environ. Manage.*, 50, 721-735, [https://doi.org/10.1007/s00267-012-9921-](https://doi.org/10.1007/s00267-012-9921-7)  
739 7, 2012.
- 740 Harris, C., Davies, M. C. R., and Etzelmüller, B.: The assessment of potential geotechnical hazards associated with  
741 mountain permafrost in a warming global climate, *Permafrost Periglac.*, 12, 145-156, <https://doi.org/10.1002/ppp.376>,  
742 2001.
- 743 Huang, F., Yin, K., Huang, J., Gui, L., and Wang, P.: Landslide susceptibility mapping based on self-organizing-map  
744 network and extreme learning machine, *Eng. Geol.*, 223, 11-22, <https://doi.org/10.1016/j.enggeo.2017.04.013>, 2017.
- 745 Iqbal, J., Dai, F., Hong, M., Tu, X., and Xie, Q.: Failure Mechanism and Stability Analysis of an Active Landslide in the  
746 Xiangjiaba Reservoir Area, Southwest China, *J. Earth Sci.*, 29, 646-661, <https://doi.org/10.1007/s12583-017-0753-5>,  
747 2018.
- 748 Karli, F., Atasoy, M., Yalcin, A., Reis, S., Demir, O., and Gokceoglu, C: Effects of land-use changes on landslides in a  
749 landslide-prone area (Ardesen, Rize, NE Turkey), *Environ. Monit. Assess.*, 156, 241-255, [https://doi.org/10.1007/](https://doi.org/10.1007/s10661-008-0481-5)  
750 s10661-008-0481-5, 2009.
- 751 Kayastha, P.: Landslide susceptibility mapping and factor effect analysis using frequency ratio in a catchment scale: a case  
752 study from Garuwa sub-basin, East Nepal, *Arab. J. Geosci.*, 8, 8601-8613, [https://doi.org/10.1007/s12517-015-1831-](https://doi.org/10.1007/s12517-015-1831-6)  
753 6, 2015.
- 754 Lee, S., Ryu, J. H., Won, J. S., and Park, H. J.: Determination and application of the weights for landslide susceptibility  
755 mapping using an artificial neural network, *Eng. Geol.*, 71, 289-302, [https://doi.org/10.1016/S0013-7952\(03\)00142-](https://doi.org/10.1016/S0013-7952(03)00142-X)  
756 X, 2004.
- 757 Lee, S.: Application of logistic regression model and its validation for landslide susceptibility mapping using GIS and  
758 remote sensing data, *Int. J. Remote Sens.*, 26, 1477-1491, <https://doi.org/10.1080/01431160412331331012>, 2005.
- 759 Lopez-Saez, J., Corona, C., Eckert, N., Stoffel, M., Bourrier, F., and Berger, F.: Impacts of land-use and land-cover changes  
760 on rockfall propagation: Insights from the Grenoble conurbation, *Sci. Total Environ.*, 547, 345-355,  
761 <https://doi.org/10.1016/j.scitotenv.2015.12.148>, 2016.



- 762 Lombardo, L., and Mai, P. M.: Presenting logistic regression-based landslide susceptibility results, *Eng. Geol.*, 244, 14-24,  
763 <https://doi.org/10.1016/j.enggeo.2018.07.019>, 2018.
- 764 Mao, Z., Yang, M., Bourrier, F., and Fourcaud, T.: Evaluation of root reinforcement models using numerical modelling  
765 approaches, *Plant Soil*, 382, 249-270, <https://doi.org/10.1007/s11104-014-2116-7>, 2014.
- 766 Mashimbye, Z. E., Clercq, W. P., and Niekerk, A. V.: An evaluation of digital elevation models (DEMs) for delineating  
767 land components, *Geoderma*, 213, 312-319, <https://doi.org/10.1016/j.geoderma.2013.08.023>, 2014.
- 768 Melchiorre, C., Matteucci, M., Azzoni, A., and Zanchi, A.: Artificial neural networks and cluster analysis in landslide  
769 susceptibility zonation, *Geomorphology*, 94, 379-400, <https://doi.org/10.1016/j.geomorph.2006.10.035>, 2008.
- 770 Meneses, B. M., Pereira, S., and Reis, E.: Effects of different land use and land cover data on the landslide susceptibility  
771 zonation of road networks, *Nat. Hazards Earth Syst. Sci.*, 19, 471-487, <https://doi.org/10.5194/nhess-19-471-2019>,  
772 2019.
- 773 Mohammady, M., Pourghasemi, H. R., and Pradhan, B.: Landslide susceptibility mapping at Golestan Province, Iran: A  
774 comparison between frequency ratio, Dempster–Shafer, and weights-of-evidence models, *J. Asian Earth Sci.*, 61, 221-  
775 236, <https://doi.org/10.1016/j.jseaes.2012.10.005>, 2012.
- 776 Nandi, A., and Shakoor, A.: A GIS-based landslide susceptibility evaluation using bivariate and multivariate statistical  
777 analyses, *Eng. Geol.*, 110, 11-20, <https://doi.org/10.1016/j.enggeo.2009.10.001>, 2009.
- 778 Ozdemir, A., and Altural, T.: A comparative study of frequency ratio, weights of evidence and logistic regression methods  
779 for landslide susceptibility mapping: Sultan Mountains, SW Turkey, *J. Asian Earth Sci.*, 64, 180-197,  
780 <https://doi.org/10.1016/j.jseaes.2012.12.014>, 2013.
- 781 Piacentini, D., Troiani, F., Soldati, M., Notarnicola, C., Savelli, D., Schneiderbauer, S., and Strada, C.: Statistical analysis  
782 for assessing shallow-landslide susceptibility in South Tyrol (south-eastern Alps, Italy), *Geomorphology*, 151-152,  
783 196-206, <https://doi.org/10.1016/j.geomorph.2012.02.003>, 2012.
- 784 Pinyol, N. M., Alonso, E. E., Corominas, J., and Moya, J.: Canelles landslide: modeling rapid drawdown and fast potential  
785 sliding, *Landslides*, 9, 33-51, <https://doi.org/10.1007/s10346-011-0246-x>, 2012.
- 786 Promper, C., Gassner, C. H., and Glade, T.: Spatiotemporal patterns of landslide exposure – a step within future landslide  
787 risk analysis on a regional scale applied in Waidhofen/YBBs Austria, *Int. J. Disast. Risk Re.*, 12, 25-33,  
788 <https://doi.org/10.1016/j.ijdr.2014.11.003>, 2015.
- 789 Pisano, L., Zumpano, V., Malek, Ž., Rosskopf, C. M., and Parise, M.: Variations in the susceptibility to landslides, as a



- 790 consequence of landcover changes: A look to the past, and another towards the future, *Sci. Total Environ.*, 601-602,  
791 1147-1159, <https://doi.org/10.1016/j.scitotenv.2017.05.231>, 2017.
- 792 Pourghasemi, H. R., and Rossi, M.: Landslide susceptibility modeling in a landslide prone area in Mazandarn Province,  
793 north of Iran: a comparison between GLM, GAM, MARS, and M-AHP methods, *Theor. Appl. Climatol.*, 130, 609-  
794 633, <https://doi.org/10.1007/s00704-016-1919-2>, 2017.
- 795 Razavizadeh, S., Solaimani, K., Massironi, M., and Kaviani, A.: Mapping landslide susceptibility with frequency ratio,  
796 statistical index, and weights of evidence models: a case study in northern Iran, *Environ. Earth Sci.*, 76, 499-514,  
797 <https://doi.org/10.1007/s12665-017-6839-7>, 2017.
- 798 Regmi, A. D., Devkota, K. C., Yoshida, K., Pradhan, B., Pourghasemi, H. R., Kumamoto, T., and Akgun, A.: Application  
799 of frequency ratio, statistical index, and weights-of-evidence models and their comparison in landslide susceptibility  
800 mapping in central Nepal Himalaya, *Arab. J. Geosci.*, 7, 725-742, <https://doi.org/10.1007/s12517-012-0807-z>, 2014.
- 801 Regmi, N. R., Giardino, J. R., and Vitek, J. D.: Assessing susceptibility to landslides: Using models to understand observed  
802 changes in slopes, *Geomorphology*, 122, 25-38, <https://doi.org/10.1016/j.geomorph.2010.05.009>, 2010.
- 803 Reichenbach, P., Busca, C., Mondini, A. C., and Rossi, M.: The influence of land use change on landslide susceptibility  
804 zonation: the Briga Catchment test site (Messina, Italy), *Environ. Manage.*, 54, 1372-1384,  
805 <https://doi.org/10.1007/s00267-014-0357-0>, 2014.
- 806 Revellino, P., Guadagno, F. M., and Hungr, O.: Morphological methods and dynamic modelling in landslide hazard  
807 assessment of the Campania Apennine carbonate slope, *Landslides*, 5, 59-70, [https://doi.org/10.1007/s10346-007-](https://doi.org/10.1007/s10346-007-0103-2)  
808 0103-2, 2008.
- 809 Rotigliano, E., Cappadonia, C., Conoscenti, C., Costanzo, D., and Agnesi, V.: Slope units-based flow susceptibility model:  
810 using validation tests to select controlling factors, *Nat. Hazards*, 61, 143-153, [https://doi.org/10.1007/s11069-011-](https://doi.org/10.1007/s11069-011-9846-0)  
811 9846-0, 2012.
- 812 Scalenghe, R., and Marsan, F. A.: The anthropogenic sealing of soils in urban areas. *Landscape Urban Plan.*, 90, 1-10,  
813 <https://doi.org/10.1016/j.landurbplan.2008.10.011>, 2009.
- 814 Schlögel, R., Marchesini, I., Alvioli, M., Reichenbach, P., Rossi, M., and Malet, J. P.: Optimizing landslide susceptibility  
815 zonation: Effects of DEM spatial resolution and slope unit delineation on logistic regression models, *Geomorphology*,  
816 301, 10-20, <https://doi.org/10.1016/j.geomorph.2017.10.018>, 2018.
- 817 Schmaltz, E. M., Steger, S., and Glade, T.: The influence of forest cover on landslide occurrence explored with spatio-



- 818 temporal information, *Geomorphology*, 290, 250-264, <https://doi.org/10.1016/j.geomorph.2017.04.024>, 2017.
- 819 Shrestha, D. P., Saepuloh, A., and Van Der Meer, F.: Land cover classification in the tropics, solving the problem of cloud  
820 covered areas using topographic parameters, *Int. J. Appl. Earth Obs.*, 77, 84-93. [https://doi.org/10.1016/j.jag.2018.](https://doi.org/10.1016/j.jag.2018.12.010)  
821 12.010, 2019.
- 822 Tasser, E., Mader, M., and Tappeiner, U.: Basic and applied ecology effects of land use in alpine grasslands on the  
823 probability of landslides, *Basic Appl. Ecol.*, 280, 271-280, <https://doi.org/10.1078/1439-1791-00153>, 2003.
- 824 Taubenböck, H., Wurm, M., Netzband, M., Zwenzner, H., Roth, A., Rahman, A., and Dech, S.: Flood risks in urbanized  
825 areas – multi-sensorial approaches using remotely sensed data for risk assessment, *Nat. Hazards Earth Syst. Sci.*, 11,  
826 431-444, <https://doi.org/10.5194/nhess-11-431-2011>, 2011.
- 827 Tian, Y., Xu, C., Ma, S., Wang, S., and Zhang, H.: Inventory and Spatial Distribution of Landslides Triggered by the 8th  
828 August 2017 MW 6.5 Jiuzhaigou Earthquake, China, *J. Earth Sci.*, 30, 206-217, [https://doi.org/10.1007/s12583-018-](https://doi.org/10.1007/s12583-018-0869-2)  
829 0869-2, 2019.
- 830 Van Den Eeckhaut, M., Reichenbach, P., Guzzetti, F., Rossi, M., and Poesen, J.: Combined landslide inventory and  
831 susceptibility assessment based on different mapping units: an example from the Flemish Ardennes, Belgium, *Nat.*  
832 *Hazards Earth Syst. Sci.*, 9, 507-521, <https://doi.org/10.5194/nhess-9-507-2009>, 2009.
- 833 Van Westen, C. J., van Asch, T. W. J., and Soeters, R.: Landslide hazard and risk zonation—why is it still so difficult? *Bull.*  
834 *Eng. Geol. Environ.*, 65, 167-184, <https://doi.org/10.1007/s10064-005-0023-0>, 2006.
- 835 Van Westen, C. J., Castellanos, E., and Kuriakose, S. L.: Spatial data for landslide susceptibility, hazard, and vulnerability  
836 assessment: An overview, *Eng Geol.*, 102, 112-131, <https://doi.org/10.1016/j.enggeo.2008.03.010>, 2008.
- 837 Vasu, N. N., and Lee, S. R.: A hybrid feature selection algorithm integrating an extreme learning machine for landslide  
838 susceptibility modeling of Mt. Woomyeon, South Korea, *Geomorphology*, 263, 50-70, [https://doi.org/10.1016/](https://doi.org/10.1016/j.geomorph.2016.03.023)  
839 [j.geomorph.2016.03.023](https://doi.org/10.1016/j.geomorph.2016.03.023), 2016.
- 840 Wang, F., Yin, K. Gui, L., and Chen, L.: Risk Analysis on Individual Reservoir Bank Landslide and Its Generated Wave,  
841 *Earth Sci.*, 43, 899-909 (in Chinese with English abstract), <https://doi.org/10.3799/dqkx.2018.910>, 2018.
- 842 Xie, M., Esaki, T., and Zhou, G.: GIS-based probabilistic mapping of landslide hazard using a three-dimensional  
843 deterministic model, *Nat. Hazards*, 33, 265-282, <https://doi.org/10.1023/B:NHAZ.0000037036.01850.0d>, 2004.
- 844 Yalcin, A., Reis, S., Aydinoglu, A. C., and Yomralioglu, T. A.: GIS-based comparative study of frequency ratio, analytical  
845 hierarchy process, bivariate statistics and logistics regression methods for landslide susceptibility mapping in Trabzon,



- 846 NE Turkey, *Catena*, 85, 274-287, <https://doi.org/10.1016/j.catena.2011.01.014>, 2011.
- 847 Ymeti, I., Van Der Werff, H., Shrestha, D. P., Jetten, V. G., Lievens, C., and Van Der Meer, F.: Using color, texture and  
848 objected-based image analysis of multi-temporal camera data to monitor soil aggregate breakdown, *Sensors*, 17, 1241-  
849 1261, <https://doi.org/10.3390/s17061241>, 2017.
- 850 Zhang, T., and Tang, H.: A Comprehensive Evaluation of Approaches for Built-Up Area Extraction from Landsat OLI  
851 Images Using Massive Samples, *Sensors*, 11, 2-13, <https://doi.org/10.3390/rs11010002>, 2019.
- 852 Zhou, C., Yin, K., Cao, Y., Ahmed, B., Li, Y., Catani, F., and Pourghasemi, H. R.: Landslide susceptibility modeling  
853 applying machine learning methods: A case study from Longju in the Three Gorges Reservoir area, China, *Comput.*  
854 *Geosci.*, 112, 23-37, <https://doi.org/10.1016/j.cageo.2017.11.019>, 2018